NOTE TO USERS

This reproduction is the best copy available.

UMI®

A Computational Thermodynamic Model of the Mg-Al-Y System

Saher Al Shakhshir

A Thesis

In

The Department

of

Mechanical and Industrial Engineering

Presented in Partial Fulfillment of the Requirements
for the Degree of Master of Applied Science (Mechanical Engineering) at
Concordia University
Montreal, Quebec, Canada

August 2005

© Saher Al Shakhshir, 2005

Library and Archives Canada

Published Heritage Branch

395 Wellington Street
Ottawa ON K1A 0N4
Canada

Bibliothèque et Archives Canada

Direction du Patrimoine de l'édition

395, rue Wellington
Ottawa ON K1A 0N4
Canada

Your file Votre référence
ISBN: 0-494-10262-4
Our file Notre référence
ISBN: 0-494-10262-4

NOTICE:
The author has granted a non-exclusive license allowing Library and Archives Canada to reproduce, publish, archive, preserve, conserve, communicate to the public by telecommunication or on the Internet, loan, distribute and sell theses worldwide, for commercial or non-commercial purposes, in microform, paper, electronic and/or any other formats.

The author retains copyright ownership and moral rights in this thesis. Neither the thesis nor substantial extracts from it may be printed or otherwise reproduced without the author's permission.

AVIS:
L'auteur a accordé une licence non exclusive permettant à la Bibliothèque et Archives Canada de reproduire, publier, archiver, sauvegarder, conserver, transmettre au public par télécommunication ou par l'Internet, prêter, distribuer et vendre des thèses partout dans le monde, à des fins commerciales ou autres, sur support microforme, papier, électronique et/ou autres formats.

L'auteur conserve la propriété du droit d'auteur et des droits moraux qui protège cette thèse. Ni la thèse ni des extraits substantiels de celle-ci ne doivent être imprimés ou autrement reproduits sans son autorisation.

In compliance with the Canadian Privacy Act some supporting forms may have been removed from this thesis.

While these forms may be included in the document page count, their removal does not represent any loss of content from the thesis.

Conformément à la loi canadienne sur la protection de la vie privée, quelques formulaires secondaires ont été enlevés de cette thèse.

Bien que ces formulaires aient inclus dans la pagination, il n'y aura aucun contenu manquant.

Canada

ABSTRACT

Saher Al Shakhshir

The ternary system Mg-Al-Y was thermodynamically modeled based on the optimization of the binary sub-systems Mg-Al, Mg-Y and Al-Y using the CALPHAD approach. Mg-Al data was taken from the COST507 database, whereas the other two binary sub-systems were reoptemised in this work. Liquid phases were described by the Redlich-Kister polynomial model, whereas the intermediate solid solutions were described by the sublattice model.

Ternary interaction parameters were introduced to enable the best representation of the experimental data while considering the occurrence of the ternary compound Al_4MgY. The constructed database is used to calculate and predict thermodynamic properties, binary phase diagrams of Al-Y and Mg-Y, and liquidus projections of the ternary Mg-Al-Y. The phase diagrams and the thermodynamic properties calculated with the evaluated parameters were in good agreement with the corresponding experimental data from the literature. The predicted invariant points in the Mg-Al-Y system were 16 ternary four-phase-equilibria points; 7 ternary eutectic points, 8 ternary quasi peritectic points, and one ternary peritectic point. Further, 15 ternary three-phase-equilibria points were determined; 8 saddle points, and 7 binary eutectic points.

ACKNOWLEDGEMENTS

First of all I would like to thank my family for their endless love and support, who first encouraged me to apply and come to Concordia University, especially my parents, who contacted me always, and encouraged my studies.

I would like to express my deep sense of gratitude to my supervisor Dr.Medraj who offered me an opportunity to be a graduate student at Concordia University, and conduct research under his guidance. There is little I can say to add to his already impeccable reputation as a researcher and teacher. I am really indebted to him, for his constant support.

I would like to thank Hani Al Quddumi Scholarship Foundation (HQSF) for their financial suppor. And I thank Concordia University for providing fantastic facilities and a comfortable and relaxing environment, which enabled me to focus my attention on my research.

I thank the fellow graduate students in my office, who provided me with a perfect research environment with all the fun and offered support whenever needed. Especially, I thank Thevika Thangarajah, Farhana Islam, and Muhammad Ashraf -ul- Arafin for their help and support during my research.

I thank all staff members of our department for their kind help in solving my academic and technical problems. Especially, I would like to thank Andie Zeliger who was very helpful and supportive. Special thanks also for the IT group in Mechanical Engineering department, who helped in installing the required programs in keeping them running.

Finally, I would like to acknowledge the help of my friends Khassan Mourtazov and Amr Abu Samaan who helped me in translation of some articles from Russian to English. This was a great assistant for me. Also, I thank Amer Samara who provided the greatest support and help when they were needed the most.

TABLE OF CONTENTS

LIST OF FIGURES

LIST OF TABLES

NOMENCLATURE

G	Gibbs energy in J
${}^{0}G_i^{\phi}$	Standard Gibbs energy of ϕ phase
G_i^{ϕ}	Gibbs energy of ϕ phase
ΔG_f	Gibbs energy of formation change
${}^{ex}G^{\phi}$	Excess Gibbs energy of ϕ phase
$\Delta H_f 298.15$	Heat of formation at 25 °C
ΔH	Enthalpy change
H^{SER}	Molar enthalpy of the stable element
${}^{n}L^{\phi}_{ij}$	Empirical coefficients for Redlich-Kister polynomial expansion
p	Number of phases
T	Temperature
R	Gas constant
x	Mole fraction

CHAPTER1

INTRODUCTION

1.1 THERMODYNAMICS OF PHASE DIAGRAMS

Since the earliest use of phase diagrams, scientists and engineers have found them very useful in describing the different forms a certain material can take. By examining a phase diagram one can gain some understanding into mechanical properties of a material. Therefore knowledge of phase diagrams plays an important role in the development, processing, and application of materials. In addition, phase diagrams provide a road map for materials design and process optimization since it is the starting point in manipulation and calculation of processing variables to achieve the desired microstructure [1].

Modern materials are often multicomponent, thus making their phase diagrams quite complex. Experimental determination of such phase diagrams can be time-consuming, expensive, and difficult. Therefore, one is usually faced with the fact that the required phase diagram is not available. The CALPHAD (CALculation of PHAse Diagrams) method offers a reliable and versatile alternative to generate phase diagrams, and requires only less experimental data compared to the conventional methods [2]. In this approach, the required Gibbs energy functions are usually obtained by employing computational thermodynamics considering both the experimental thermochemical and constitutional data from the related literature. There are few commercial software that can

be used for this purpose, most of which were classified as first generation software by Chang *et al.* [3]. However, PANDAT software was classified an introduction to second generation software [3]. The present research focuses on thermodynamic modeling of the multicomponent Mg-Al-Y alloy system based on the CALPHAD method using PANDAT software [4].

1.2 Mg-Al-Y Ternary SYSTEM

A ternary system is represented onto an equilateral triangle base (Gibbs triangle) representing the composition, and the temperature is given along the vertical axis. However, the pressure is constant and it is 1 atm in this study. For example the hypothetical ternary system of A-B-C alloy is shown in Figure 1.1(a). The liquidus surfaces are projected onto the composition triangle as shown in Figure 1.1 (b).

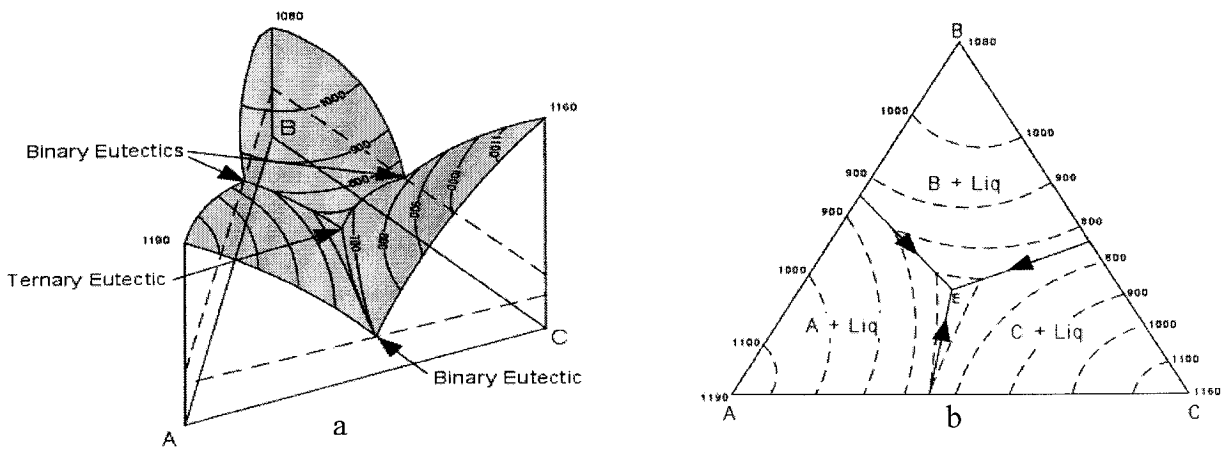

***Figure 1.1**: A-B-C ternary system (a) three dimensional representation, (b) projection of the liquidus surface onto the composition triangle [5].*

Calculating and constructing the A-B-C ternary phase diagram requires a deep understanding and accurate calculation for the binaries A-B, A-C, and B-C which

represent the three faces of the most prism. These binaries are simple eutectic, and it gives a ternary phase diagram with three liquidus surfaces which intersect at the ternary eutectic point as shown in Figure 1.1(a). Therefore, calculating and constructing the Mg-Al-Y system requires a comprehensive study and accurate mathematical representation of all phases in the constituent binaries: Mg-Al, Al-Y, and Mg-Y [6].

1.3 THE IMPORTANCE OF THE Mg-Al-Y SYSTEM

Vehicle weight reduction is one of the most efficient ways to reduce automotive fuel consumption. High-strength steels, aluminum (Al), and polymers are already being used to reduce weight significantly, but considerable additional reductions could be achieved by greater use of low-density magnesium (Mg) and its alloys [7]. However, the use of magnesium alloys has been restricted due to their poor mechanical properties and its ignition behavior at high temperature.

Most magnesium commercial products are being made out of the standard magnesium die-casting alloy AZ91 (Mg- 9.5 Al- 0.5 Zn- 0.3 Mn, wt%). This alloy has excellent castability and shows good corrosion resistance with respect to other commercial Mg-alloys. However, it suffers from low mechanical properties and low creep resistance at high temperature [8], and it ignites at 590°C which makes it inappropriate for many of the components in automobile engines [9]. Therefore, new magnesium alloys are needed to meet the automobile and aerospace requirements for elevated temperature, high strength, and high creep resistance applications.

Mg-Al-Y alloy is one of the newly developed magnesium alloys. Al is an important alloying element in die-cast Mg alloys due to its strong effects on improving the strength at ambient temperatures, the corrosion resistance and the castability of the alloys. Yttrium additions in Mg alloys usually bring about alloy strengthening at elevated temperatures [10,11]. It is therefore of great interest to investigate the Mg-Al-Y system to obtain better understanding of the alloying behavior of Y in Mg-Al alloys.

Socjusz Podosek and Litynsk *et al.* [10] studied the effect of adding yttrium to Mg alloys. They reported that adding yttrium to Mg alloys will improve the mechanical properties of these alloys as shown in Table 1.1.

***Table 1.1**: Effect of yttrium content on the mechanical properties of Mg-Alloys [10]*

Alloy (Wt %)	Compression Test (Mpa)	Hardness (HV_5)
AZ91D		54*
Mg-2Y	51	68
Mg-4Y	72	75
Mg-6Y	109	90

measured at different conditions [8]

The strengthening mechanism responsible for increasing the mechanical properties of the Mg-alloys is solution hardening. This mechanism is due to the large atomic misfit between Mg and Y atoms. Figure 1.2 presents a Back Scattered Electron image (BSE) of the Mg-6Y alloy, the lighter areas along grain boundaries indicate the presence of an increased amount of Y.

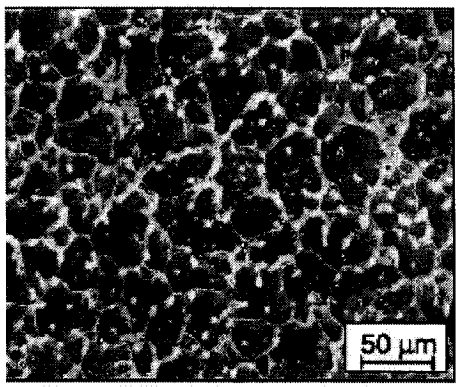

Figure 1.2: *BSE image showing the dendritic morphology of the Mg-6Y alloy [10]*

Figure 1.3 shows that creep resistance at elevated temperature increases by increasing the yttrium content in Mg-alloys [11].

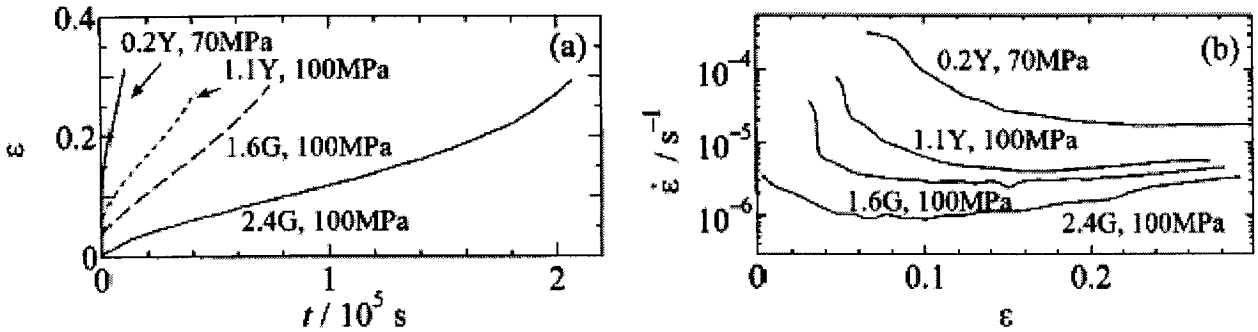

Figure 1.3*: Typical creep curves of Mg-alloys at 550 K. (a) strain time curves (b) strain rate-strain curves [11] G refers to alloys aged in air to obtain stable microstructures.*

Two strengthening mechanisms besides the solid solution hardening play a part in improving the creep resistance in Mg-alloys [11]; one is the forest-dislocation hardening due to the enhancement of the non basal slip systems. This mechanism is enhanced linearly with increasing yttrium contents. With higher yttrium concentration contents the second strengthening mechanism is dynamic precipitation. The large increase in strength at high yttrium contents is due to this extra contribution of the dynamic precipitation [11].

Ignition is one of the most common problems which face Mg alloys beyond their melting point. Adding yttrium to Mg-alloys increases the ignition resistance significantly. Ravi Kumar *et al.* [9] studied the ignition behavior of various Mg alloys experimentally. They investigated the pure Mg, AZ91 (Mg- 9.5 Al- 0.5 Zn- 0.3 Mn, wt%) and the WE43 (Mg -0.5 Zr -3.25 Nd -4Y, wt%) alloys.

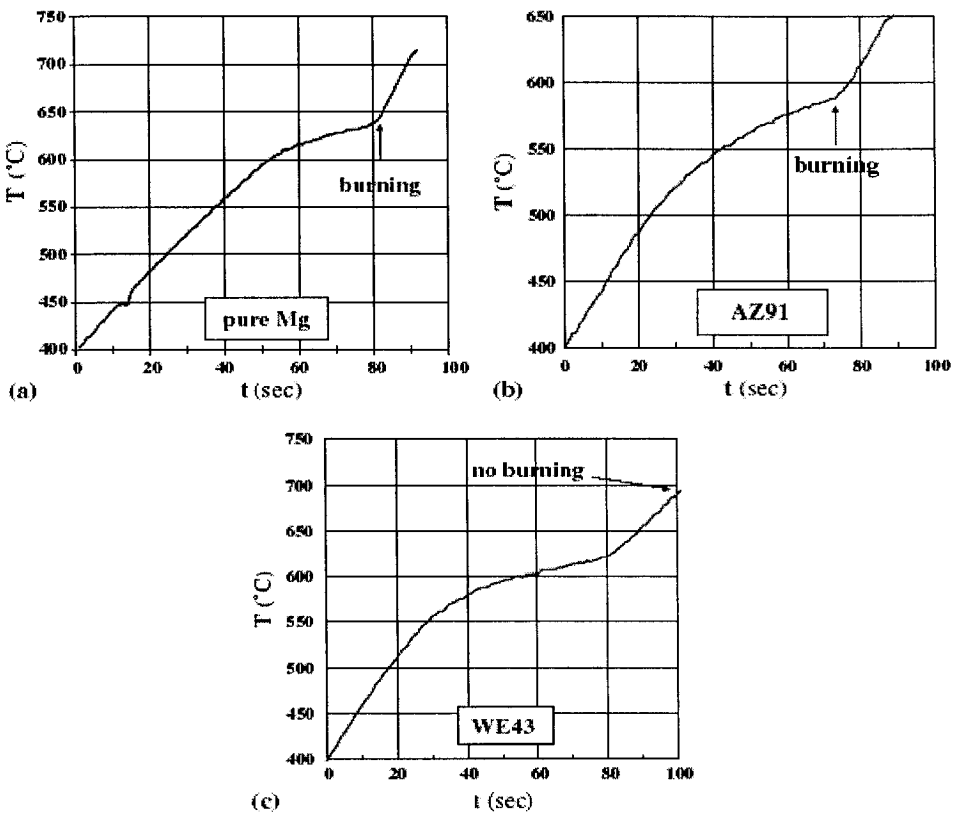

***Figure 1.4**: Ignition curves of (a) pure Mg, (b) AZ91, and (c) WE4 [9].*

In pure Mg, ignition takes place in the solid state just before melting as shown in Figure 1.4(a). Ignition of AZ91 alloy is observed at a temperature higher than the solidus temperature as shown in Figure 1.4(b). However, the yttrium-containing Mg-alloy,

WE43, shows no ignition up to 700°C as shown in Figure 1.4(c). This is attributed to the particular role of yttrium in the oxidation process. During heating, the sample oxides continuously (changing color from grey to yellowish red). When the temperature is in the semi-solid range around 600°C, the sample deforms significantly. However, the yttrium oxide sustains the strain until 650°C. At higher than 650°C the oxide film cracks, but very quickly a new oxide layer is created to prevent the extended contact between air and liquid. This behavior dominates until 750°C which is a temperature high enough for the most industrial applications.

The corrosion resistance of Al alloys can be improved by adding yttrium [12] as shown Figure1.5.

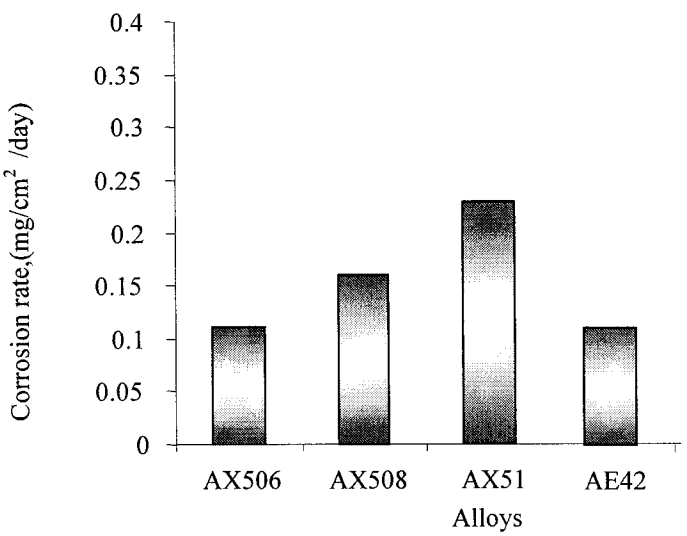

***Figure 1.5**: Effect of adding yttrium on corrosion resistance of Al-alloys [12]. AX alloys mainly contain Al and AE42 mainly contains Al and Y.*

It can be seen from Figure 1.5 that AE42 alloy has a good corrosion resistance compared with the other alloys [12]. However adding yttrium to Mg-alloys decreases the corrosion resistance. This is due to the formation of $Mg_{24}Y_5$ which behaves as an

effective cathode for the other solid solutions [13]. In general, adding the rare earth metals to Mg-alloys deteriorates corrosion resistance [14]. Nevertheless, some of these alloys still have comparable corrosion resistance to other commercial Mg-alloys. For instance, WE42 alloy (Mg-Al-RE elements) shows a better corrosion resistance than AS21 alloy and it is comparable to AZ91 as shown in Figure 1.6 [8].

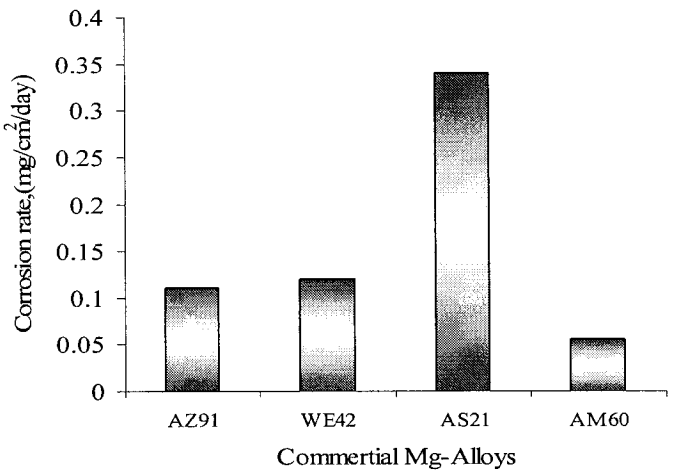

***Figure 1.6**: The corrosion resistance of the commercial Mg-alloys [8].*

1.4 OBJECTIVES

The main objective of this study is to carry out thermodynamic modeling and calculation of the ternary Mg-Al-Y system and to construct a reliable database for this system. This database will be used in thermodynamic modeling of higher order systems (e.g. Mg-Al-Ca-Y). This objective is achieved in this work through:

- Thermodynamic modeling of all phases in the binary sub-systems Al-Y and Mg-Y systems. However the thermodynamic description of the Mg-Al system, which was obtained through the COST507 [15] project, will be used in this study.

- Calculating the phase diagrams and the thermodynamic properties of Al-Y and Mg-Y systems and comparing the results with the experimental data reported in the literature.
- Thermodynamic modeling of the ternary Al_4MgY compound which occur in the ternary Mg-Al-Y system.
- Construction of a database for the Mg-Al-Y ternary alloy system by combining the thermodynamic descriptions of the constituent binaries Mg-Y, Al-Y, and Mg-Al, along with the thermodynamic model of Al_4MgY phase.
- Calculating the Mg-Al-Y ternary phase diagram from the constructed database for this system.
- Identification of the invariant points and the primary crystallization field of each phase in the Mg-Al-Y ternary system and comparing the results with the experimental data reported in the literature.
- Calculating some vertical sections from the constructed database and comparing it with available experimental data from the literature.

CHAPTER2

EXPERIMENTAL DATA EVALUATION

2.1 INTRODUCTION

The first step of thermodynamic modeling and optimization is collecting and classifying the experimental data from the literature. Basically any type of experimental data pertinent to Gibbs energy can be used as an input for the thermodynamic modeling and optimization process. Typically the constitutional and thermochemical results are the data used for this purpose and can be collected from the literature [16]. Crystallographic data is also used because it is essential for Gibbs energy modeling of the long range ordered phases.

The second step is categorized under the critical evaluation of the collected data. This evaluation eliminates the inconsistent and the contradictory experimental data. This evaluation can not be achieved by the software which performs the optimization and the calculation process. It requires considerable expertise with some knowledge of the experimental techniques which are used in materials analysis [16]. This chapter analyzes the previous research work on Al-Y, Mg-Y, and Mg-Al-Y systems.

2.1 Al-Y BINARY SYSTEM

2.1.1 Al-Y Phase Diagram data

Savitiskii *et al.* [17] were the first to investigate the Al-Y system using metallographic and thermo-analytical measurements. They reported the formation of the peritectic intermetallic compound Y_2Al_5 at 1355°C. A second compound was noticed and it was designated as Y_yAl_x. Snyder [18] studied the Al-Y system by thermal analysis, X-Ray diffraction and metallographic analysis and reported, with ±5°C accuracy, the liquidus and five intermetallic compounds: Al_2Y and Al_2Y_3 which melt congruently at 1485°C and 1100°C, respectively, and three incongruent melting compounds: Al_3Y, AlY, and AlY_2. In his work, it was found that the eutectic reactions in the Al-rich and Y-rich regions take place at 640°C and 960°C, respectively. Further, the eutectic reaction $L \leftrightarrows Al_2Y_3+AlY$ takes place at 1088°C. The peritectic reactions for Al_3Y, Al_2Y, and AlY_2 take place at 980°C, 1130°C, and 985°C respectively as shown in Figure 2.1.

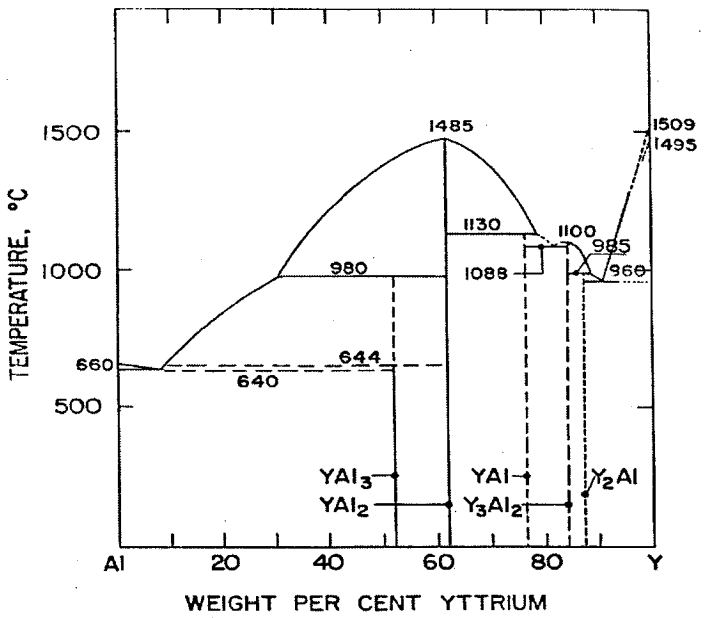

***Figure 2.1**: Proposed Al-Y phase diagram from the combination of thermal, X-Ray, and metallographic data experiments of [18], dashed line expresses the unprecisely determined borders.*

Lundin *et al.* [19] investigated this system by microstructure observations and X-ray methods and reported the phase diagram shown in Figure 2.2. Their results are in general agreement with Snyder [18] except in the following points: the solid solubility of Y in Al was less than 0.1 wt% at the eutectic temperature and the YAl_3 peritectic reaction takes place at 1355°C instead of 980°C as reported by Snyder [18], knowing that the accuracy of the reported temperature by Lundin *et al.* [19] was ±10°C.

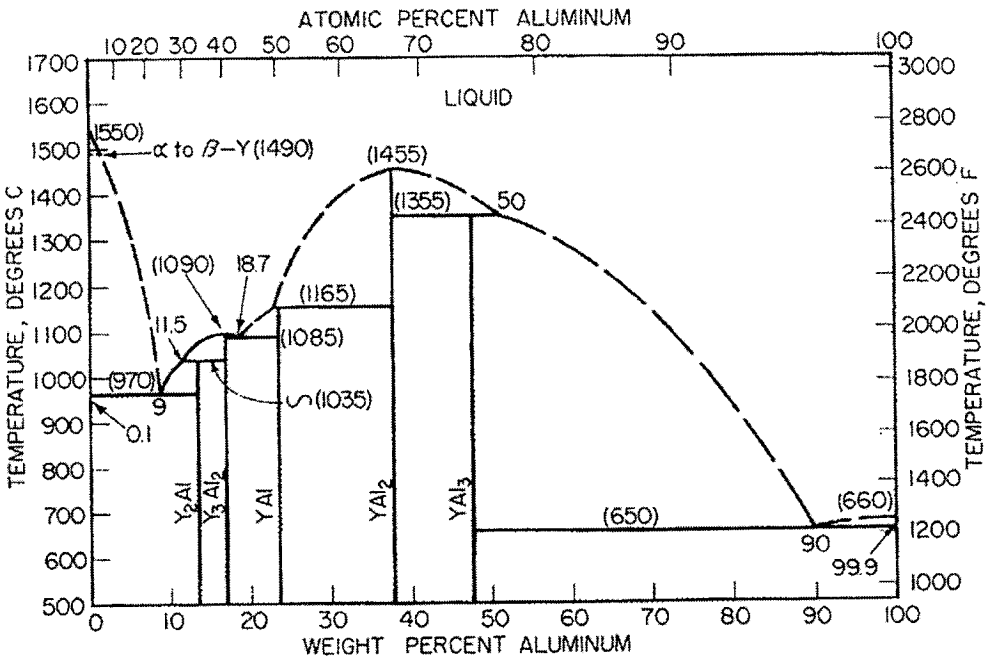

***Figure 2.2**: The equilibrium diagram of Al-Y system built from the X-ray and metallographic techniques, the dashed line represents the metallographic data [19]*

Drits *et al.* [20] investigated the Al-rich region using thermal analysis and microstructural studies. Their results were also in good agreement with [18,19]. Gscheidner *et al.* [21] assessed the Al-Y phase diagram based on the work of Snyder [18] and Lundin *et al.*[19]. They reported that βY phase melts at 1522°C and yttrium undergoes an $\alpha \leftrightarrow \beta$ allotropic phase transformation at 1478°C as shown in Figure 2.3.

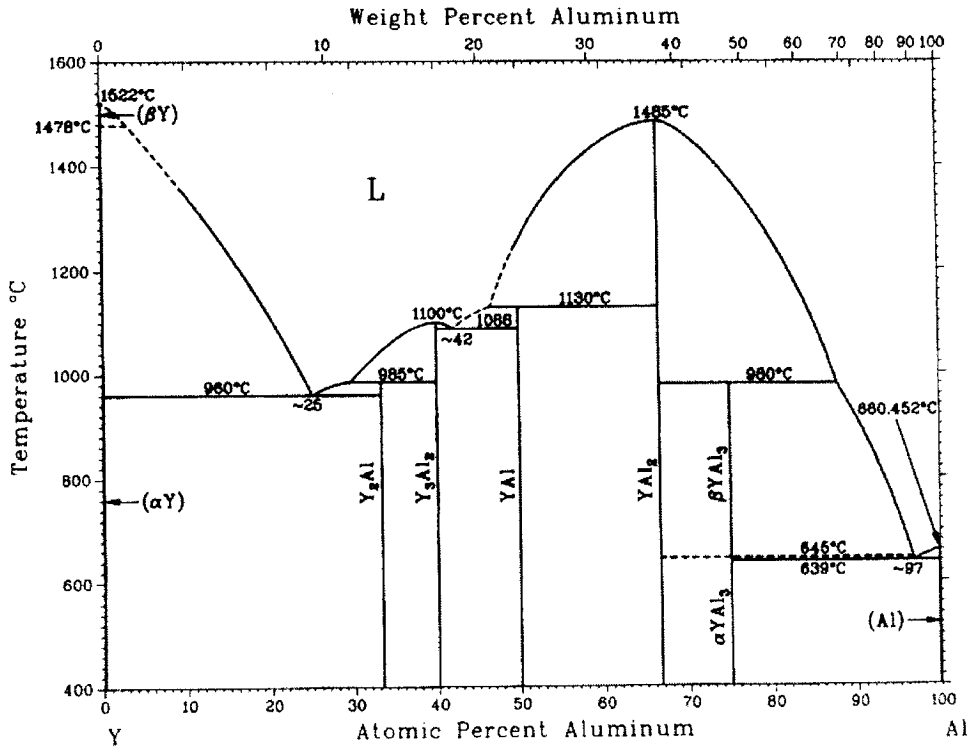

***Figure 2.3**: Calculated Y-Al phase diagram [21].*

Kripyakevich *et al.* [22] studied the Y-Al system by thermal analysis and reported the existence of another intermetallic compound; Al_4Y. However Rongzhen *et al.* [23] found that this compound does not exist in the Al-Y binary system, when they investigated the Al-Y-Sn isothermal section at room temperature by powder X-ray diffraction (XRD), differential thermal analysis (DTA), optical microscopy, electron microscopy, electron spectrum and electron probe microanalysis techniques.

Zhang and Wang [24] investigated the isothermal section of Al-Y-Sb at 527°C by powder XRD with the aid of DTA, optical microscopy and SEM. They confirmed the

existence of Al_3Y, Al_2Y, AlY, Al_2Y_3, and AlY_3. They reported AlY_3 instead of AlY_2 which contradicts with [18,19,23].

Chelkowsski *et al.* [25] found that the maximum solubility of Y in solid (Al) was less than 100 ppm using electrical and magnetic measurements and x-ray tests. Saveteskii *et al.* [17] found that the solubility of Y in Al is approximately 0.8 at.% Y at the eutectic temperature, and it was estimated to be less than 0.035 at.% Y at 300°C.

Richter *et al.* [26] identified the Y_5Al_3 compound as a D88 structure with Mn_5Si_3 prototype using TEM and XRD. They reported that Y_5Al_3 is a metastable compound and should not appear in the phase diagram. A transformation of Al_3Y from α to β was noticed by Bailey [27] at 645°C; however, the two different phases α and β were not confirmed by Raggio *et al.* [28], or by Zhang and Wang [24].

2.1.2 Thermodynamic Data

The heat of mixing and the partial enthalpies were measured by Esin *et al.* [29] and Ryss *et al.* [30] calorimetrically at 1600°C. The values reported in these two articles show a discrepancy, although they have common coauthors. This is due to the difficulty in dealing with the Al-Y system experimentally, because while adding more yttrium, the reaction becomes more exothermic.

The partial Gibbs energy of yttrium was measured by Kobber *et al.* [31] at 527°C using electromotive force (EMF) method. However, they reported unknown composition between 33 and 50 at.% Y at a certain measured values of the partial Gibbs free energy as shown in Table 2.1.

Table 2.1: *Partial Gibbs energy of Y [31].*

at.%Y	$\triangle G_Y$ (Kcal/g-atom)
0-0.25	37.9±0.1
0.05-0.33	31.3±0.1
0.33-X*	30.3±0.2
X-0.5	29.6±0.2
0.5-0.6	26.7±0.2
0.6-0.66	8.8

**** denotes undetermined composition***

Partial Gibbs energies and the heat of mixing were determined by Peterov *et al.* [32] using the vapor pressure technique. Their results show a discrepancy with the measurements of Esin *et al.* [29] and Ryss *et al.* [30]. In this work, the experimental data of the partial Gibbs energy were not used in the optimization process since the results from literature are self contradicting and some compositions were not determined as shown in Table 2.1.

The heats of formation of Al_3Y, Al_2Y, and AlY were determined calorimetrically by Snyder [18]. Gröbner *et al.* [33] reported the enthalpy of formations of AlY, Al_2Y and Al_3Y during the course of their study on the Y-Al-C system. Whereas, Timofeev *et al.* [34] determined the thermodynamic properties of Al_2Y and Al_2Y_3 using a liquid-metal solution calorimetry. Bronze *et al.* [35] used the EMF method to measure the heat of formation of the AlY and Al_2Y compounds.

Kober *et al.* [31] determined the activities of Al at 527°C using the EMF technique. Petrusheveskii and Ryss [36] reported the activity of Al and Y at 1600°C using the obtained values of heat of mixing by Ryss *et al.* [30]. Kulifeev *et al.* [37] obtained the activities by measuring the partial vapor pressures of Al above Al-Y solid alloys.

The experimental data of the phase diagram which was obtained by Snyder [18] and by Gscheidner *et al.* [21] were used in the optimization of the Al-Y system, because they are consistent with each other. However, the obtained experimental data of the phase diagram by Lundin *et al.* [19] were not used, because of the high error range in the reported temperature which was ±10°C. Moreover the heat of mixing which was obtained by Esin *et al.* [29] were used in the optimization process of this system, since it was consistent with the other thermodynamic data like the reported activities by Petrusheveskii and Ryss [36]. These experimental data were quite enough to optimize the model parameters of the system.

2.2 Mg-Y BINARY SYSTEM

2.2.1 Mg-Y Phase Diagram

Sviderskaya and Padezhnova [38] used thermal analysis to study the Mg-rich region in Mg-Y alloys. A solid solution of Y in Mg was predicted and they noticed the existence of the $Mg_{24}Y_5$ compound in the Mg rich region as shown in Figure 2.4.

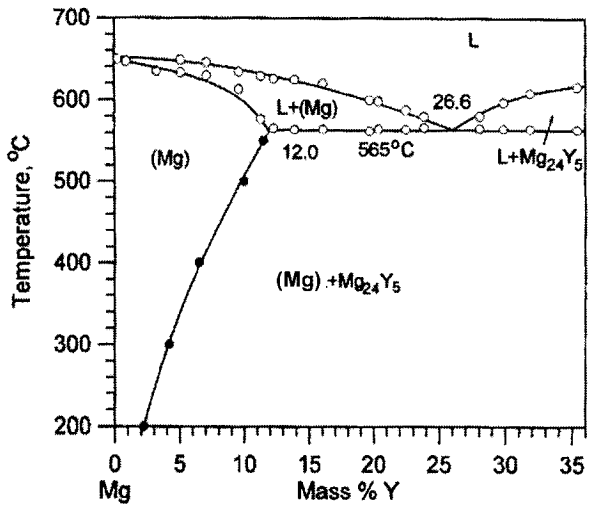

Figure 2.4: *Mg-rich region with the experimental data obtained by [38]*

Gibson and Carlson [39] investigated the Mg-Y system using thermal, microscopic, and X-ray techniques. Their work accorded with Sviderskaya and Padezhnova [38]. Three compounds; $Mg_{24}Y_5$, Mg_2Y, and MgY were formed peritectically at 60 wt% Mg, 41 wt% Mg, and 21.5wt% Mg respectively, and represented by: ε, δ, and $\gamma^{Mg\text{-}Y}$, respectively. The decomposition temperatures had been measured as 605°C, 780°C, and 935°C, respectively. A eutectic reaction was identified at 74 wt% Mg and 567°C, and a eutectoid reaction associated with an allotropic transformation in yttrium at 11 wt% Mg and 775°C. The maximum solid solubility of Y in Mg was around 9 wt% Y at 567°C as shown in Figure 2.5.

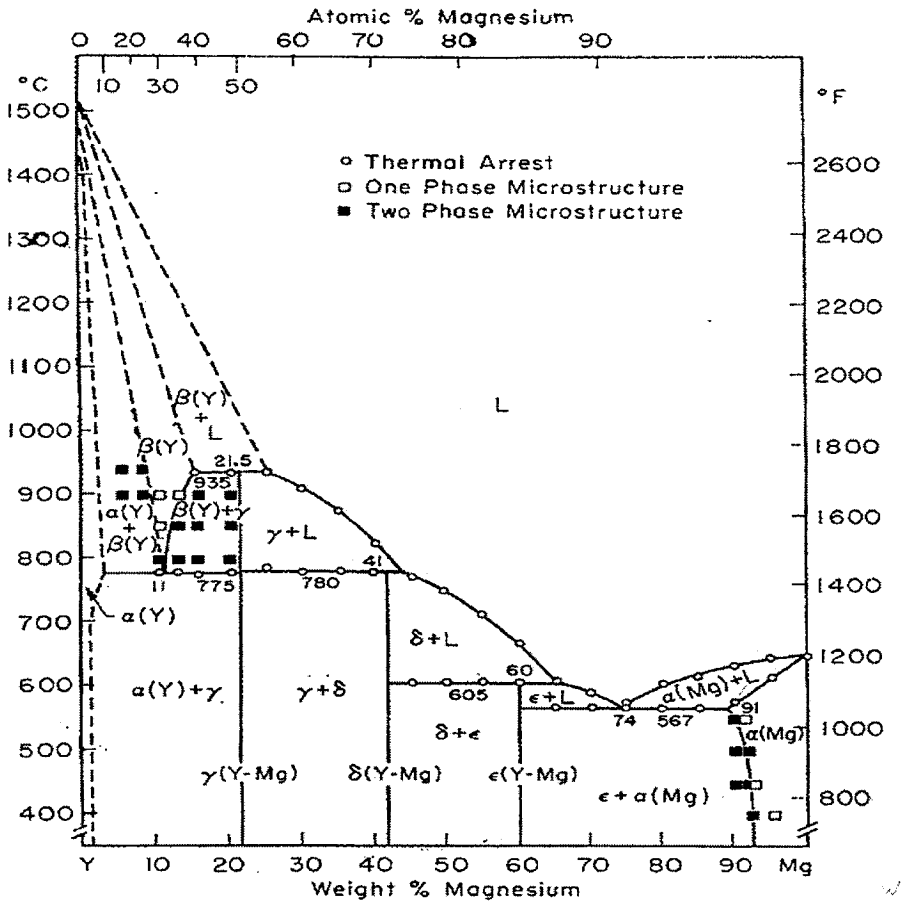

***Figure 2.5**: Proposed phase diagram with the experimental data of [39].*

Mizer and Clark [40] investigated the Mg-rich region using thermal analysis and metallography. They found that the maximum solubility of Y in solid Mg was approximately 12.6 wt% Y at the eutectic temperature 565.5°C. Their work shows a good agreement with Sviderskaya and Padezhnova [38] and Gibson and Carlson [39].

Massalski [41] assessed the Mg-Y phase diagram using the experimental work in the literature. Some modifications were applied on his results in order to comply with the results of Sviderskaya and Padezhnova [38] in the Mg-rich region as shown in Figure 2.6.

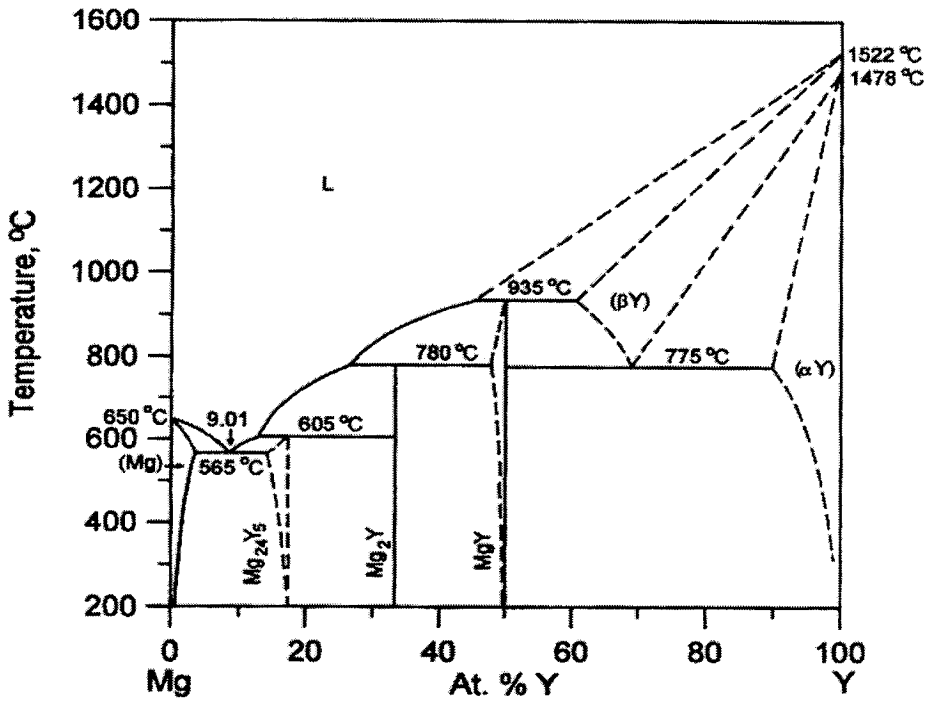

***Figure 2.6**: The estimated Mg-Y phase diagram [41].*

$Mg_{24}Y_5$ and MgY, the tangible homogeneity ranges as shown in Table 2.2 were established by X-ray investigations by Smith *et al.* [42]. The Mg_2Y phase was predicted as an intermetallic compound by [39,40,42]. This result does not agree with Flandorfer *et al.* [43], who employed XRD, optical microscopy, and microprobe analyses to study the Ce-Mg-Y isothermal section at 500°C. From their experimental work, the range of homogeneity of the Mg_2Y was obtained as shown in Table 2.2

***Table 2.2**: The homogeneity ranges of the ε, δ, and γ^{Mg-Y} -phase*

Phase	Temperatures range (°C)	Range of homogeneity at.%Y	Reference
γ^{Mg-Y}, MgY	<935	48-50	[42]
ε, $Mg_{24}Y_5$	<605	13-16	[42]
δ, Mg_2Y	<780	33.2-34.2	[43]

The crystal structures of δ, ε, and γ^{Mg-Y} were investigated using X-ray diffraction by Smith *et al.* [42]. They reported that γ^{Mg-Y} has CsCl structure, δ-phase has $MgZn_2$ structure, and ε-phase has α-Mn structure as shown in Figure 2.7. The crystallographic data will be discussed later in the modeling section of these phases in Chapter 4.

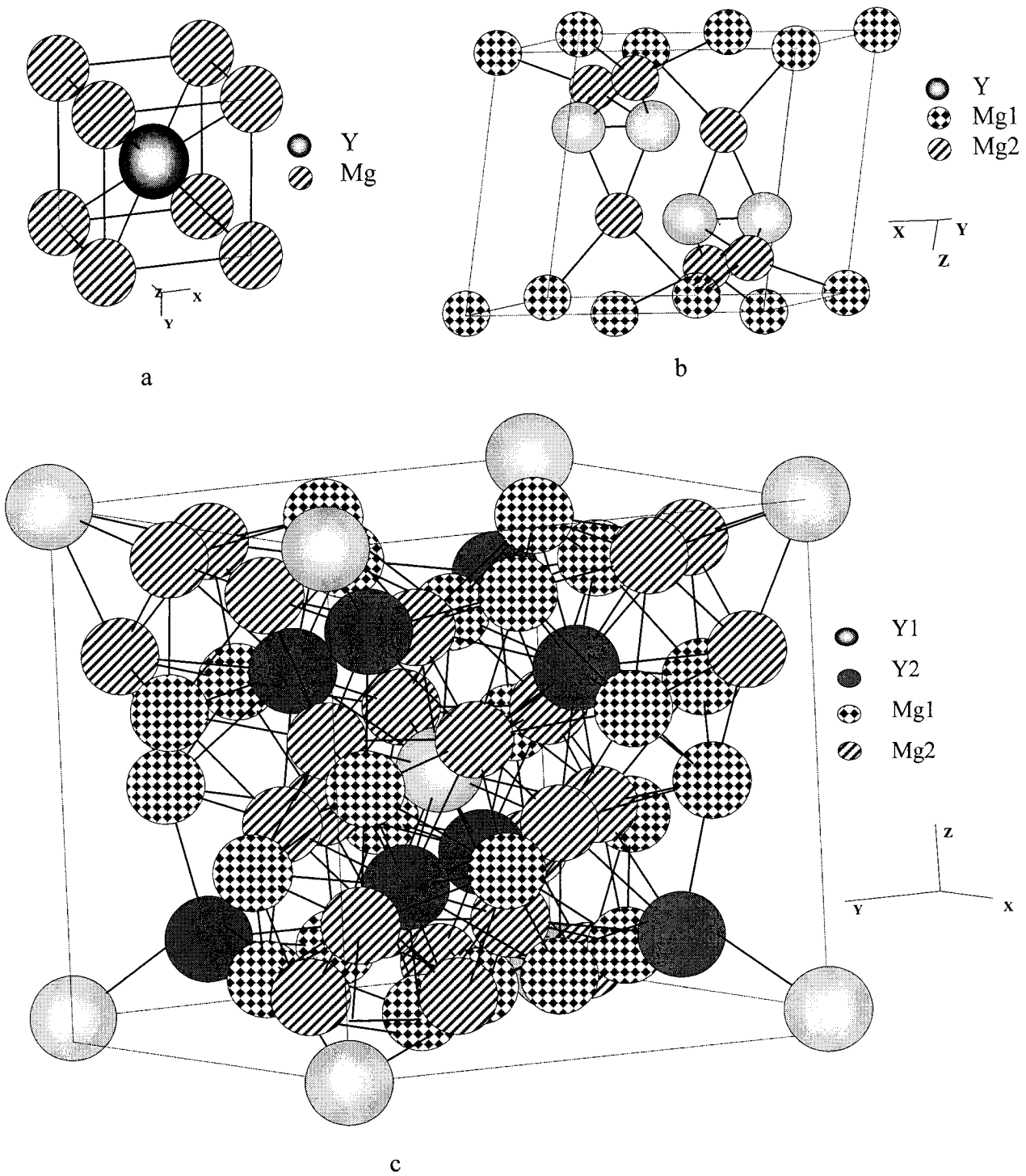

Figure 2.7: *the crystal structure of the intermediate compounds in Mg-Y alloy, (a) $\gamma^{Mg\text{-}Y}$-phase [42],(b) phase [42], and (c) δ-phase [44].*

However, the crystal structure of ε has been studied in 2004 by Zhang and Kelly [44] using TEM micrographs as shown in Figure 2.7 (c). They reported the same crystal structure as found by Smith *et al.* [42], but with one difference in the occupying atoms of the *2a* Wyckoff position. Zhang and Kelly [44] reported that this position was occupied by an Mg atom, however Smith *et al.* [42] reported that this position was occupied by 0.25 at.% Mg + 0.75 at.% Y. The work of Zhang and Kelly [44] was more precise than Smith *et al.* [42] since they used a much more advanced experimental technique for predicting the crystal structure. Therefore their results will be used in the current research.

2.2.2 Thermodynamic Data

Agrawal *et al.* [45] measured the enthalpy of mixing of liquid Mg-Y alloy in the Mg-rich region calorimetrically at different temperatures. The maximum composition attained was 21.8 at.%Y at 747°C. They extrapolated the values of the heat of mixing over the remaining composition range using the association model as shown in Figure 2.7.

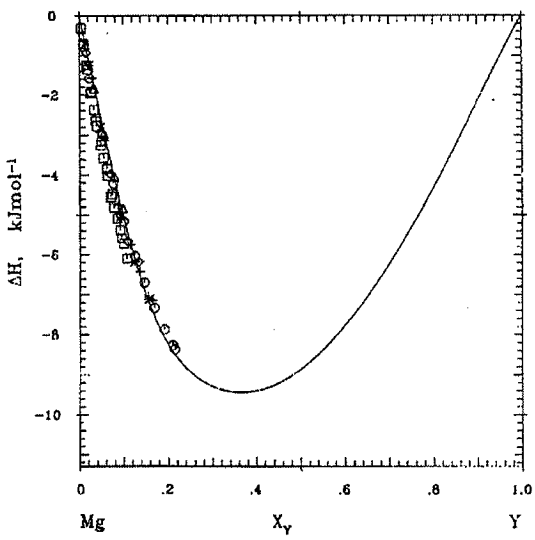

Figure 2.8: *Enthalpy of mixing of the Mg-Y liquid at 1000K, calculated by using the associated model. Experimental Data: □ 702°C, + 711°C, ◊ 682°C, Δ 801°C, * 747°C [45].*

Also, Fabrichanya *et al.* [46] calculated the heat of mixing of Mg-Y liquid alloys. Their calculations showed a good agreement with Agrawal *et al.* [45].

Activities of Mg and Y were measured by Gansen *et al.* [47] using the vapor pressure technique. Their results are in agreement with the measured activities of Mg by Isper and Gansen [48] using the same method as shown in Figure 2.9. Both results are consistent with the activities calculated by Fabrichanya *et al.* [46].

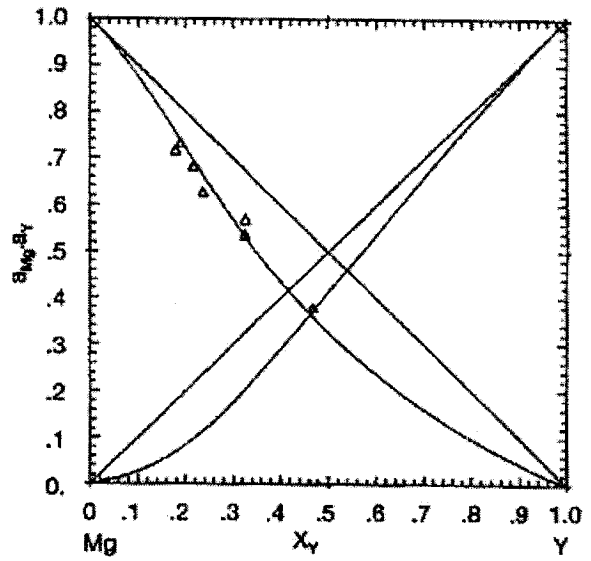

Figure 2.9: *Activities of Mg and Y at 900°C, △ experimental [48],-Calculated using the association model [47].*

Smith *et al.* [42] measured the enthalpies of formations using differential acid solution calorimetry and vapor pressure measurements. Their results are shown in Figure 2.10.

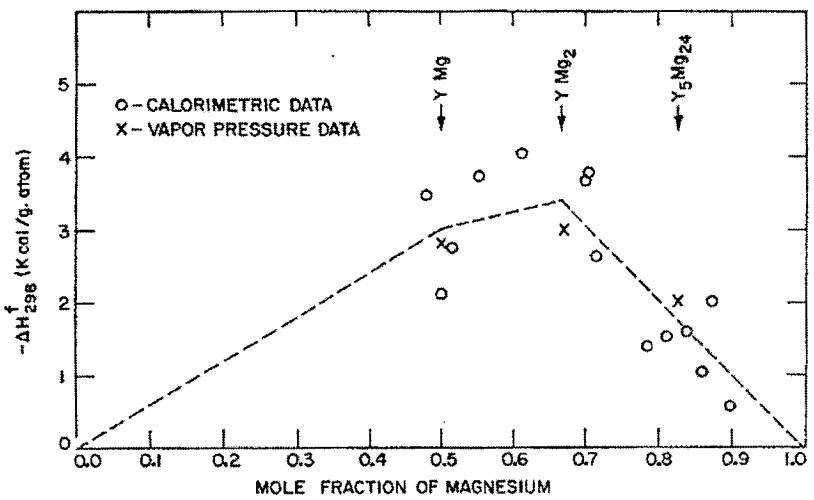

Figure 2.10: *Heat of formations as a function of composition for Mg-Y alloys [42], the dashed line represents the least square fit to the calorimetric data.*

The heat of formation of $Mg_{24}Y_5$ was measured by Smith *et al.* [42] and found consistent with the calculated value by Ran *et al.* [49]. However, the other intermediate compounds showed fair agreement between Smith *et al.* [42] and Ran *et al.* [49], This is due to the difficulties in measuring the heat of formation when the yttrium content increase and hence the reactions become more exothermic. Also, Y has a high melting point compared with Mg and this leads to sublimation of Mg during fusion of the metals [45]. Fabrichanya *et al.* [46] calculated the heat of formation and their results showed a reasonable agreement with the one measured by Smith *et al.* [42] and with the experimental data which was obtained calorimetry by Payagi *et al.* [50].

The experimental data of the Mg-Y phase diagram, which was obtained by [38,41,42] were quite enough to optimize the Mg-Y binary system. The thermodynamic experimental data were predicted by the resulting model and were in agreement with the current calculations.

2.4 Mg-Al Binary System

The literature data of this system was assessed by Thangarajah [51] a former graduate student in our research group at Concordia. She concluded that the thermodynamic model developed for this system by COST507 project [15] showed a good agreement with the experimental results of both the phase diagram as well as the thermodynamic properties. The Mg-Al calculated phase diagram using this database is shown in Figure 2.9.

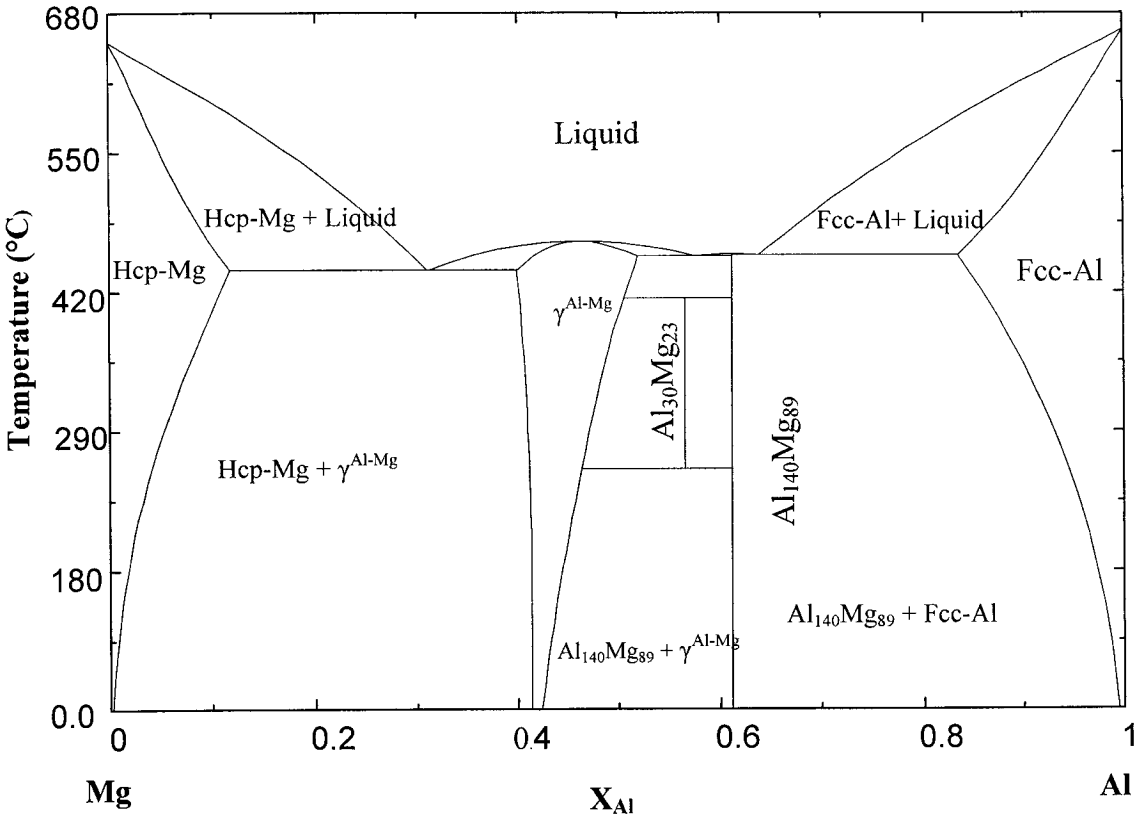

Figure 2.11: *Mg-Al phase diagram calculated using COST507 database [15]*

This system has two terminal solid solutions; Hcp-Mg and Fcc-Al, two intermetallic compounds, $Al_{30}Mg_{23}$ and $Al_{140}Mg_{89}$ and a non-stoichiometric compound $\gamma^{Mg\text{-}Al}$. The line compound $Al_{30}Mg_{23}$ is stable only in the temperature range of 250°C to 410°C. Two congruent melting compounds are identified; $\gamma^{Mg\text{-}Al}$ melts at 464°C and $Al_{140}Mg_{89}$ melts at 452°C. The first eutectic reaction is identified in the Mg-rich region at 30 at.% Mg and 435°C, the second eutectic reaction is between $\gamma^{Mg\text{-}Al}$ and $Al_{140}Mg_{89}$ at 58 at.% Mg and 448°C, and the third one is in the Al-rich region at 64 at.% Al and 450°C as shown in Figure 2.11.

2.5 Mg-Al-Y Ternary system

Drits *et al.* [52] investigated the Mg-Al-Y alloys using DTA, microscopical examination, and micro x-ray spectrum analysis. Their investigations showed that the ε ($Mg_{24}Y_5$), γ^{Mg-Al} ($Mg_{17}Al_{12}$), and Al_2Y are in equilibrium with Hcp-Mg phase in four different regions in the phase diagram.

Zarechnyuk *et al.* [53] studied this system experimentally in the range of 0 to 33 at.% Y at 400°C using x-ray diffraction, microstructure and chemical analysis. They confirmed the results which were obtained by Drits *et al.* [52]. Zarechnyuk *et al.* [53] detected for the first time the existence of τ (Al_4MgY) ternary compound. This compound was in equilibrium with Al_3Y, Al_2Y, Al_3Mg_2 and Fcc-Al in four different regions in the phase diagram. They reported that the ternary Al_4MgY compound has $MgZn_2$ crystal structure type as shown in Figure 2.12. The crystallographic data will be addressed in Chapter 4 to discuss the modeling process of this compound.

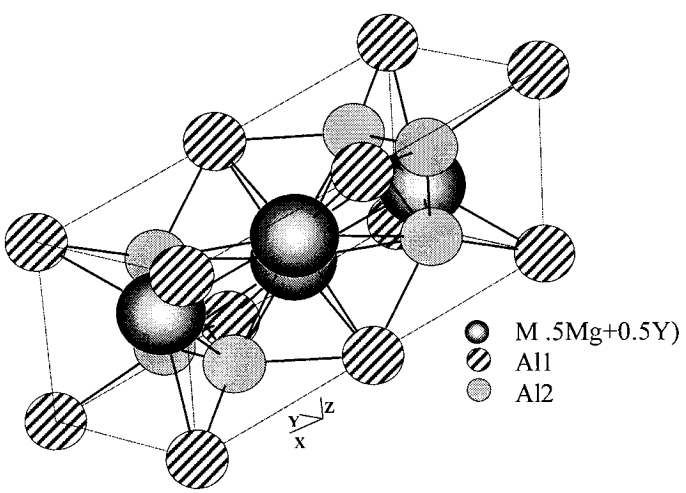

Figure 2.12: *Al_4MgY crystal structure based on the experimental results of [53].*

Odinaev and Ganiev [54] employed the XRD, metallographic analysis, and DTA to construct the liquidus surfaces and to determine the characteristic points in the Al-Mg-Al_2Y section. They confirmed the existence of τ-phase which was predicted by [53]. Their work showed that this compound is a congruent compound which melts at 750°C and the primary solidification region of τ is shown in Figure 2.13.

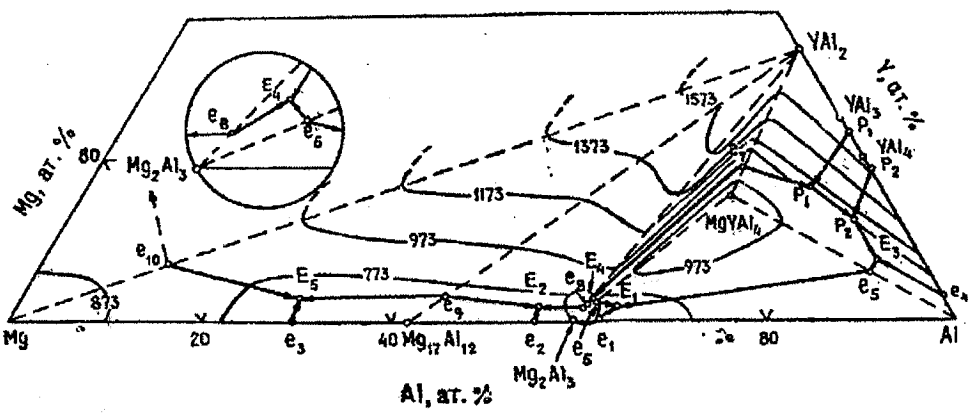

***Figure 2.13**: the experimental Mg-Al-Al_2Y ternary section with the invariant points [53].*

Odinaev *et al.* [55] constructed the Mg-Al-Y isothermal section at 400°C over the entire composition using microstructure analysis and XRD. In their work, the existence of Al_4MgY which was reported by Zarchenyuk *et al.* [53] was confirmed. Also, the existences of extensive solid solubilities between the intermetallic compounds were observed along 33.3 at.% and 50 at.% Y sections as shown in Figure 2.14.

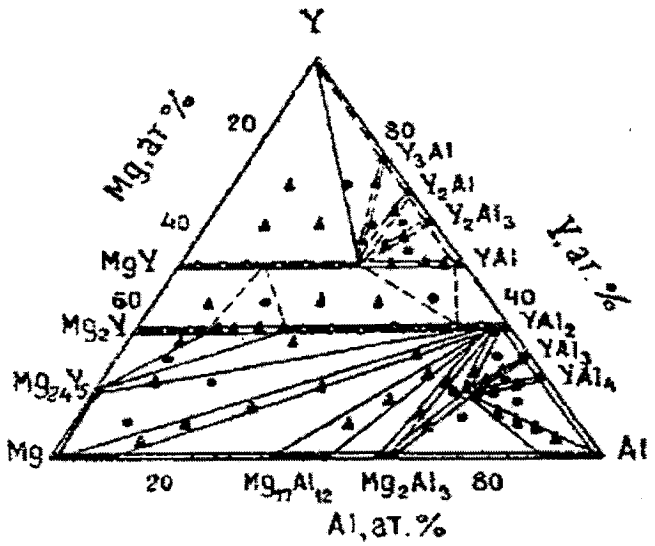

Figure 2.14: *Isothermal section of the Al-Mg-Y system at 400, – ○ single-phase alloys, ▲ two-phase alloys, ● three-phase alloys [55].*

It is worth mentioning that the existence of such extensive solid solutions was not observed by [53,54]. The results of Odinaev *et al.* [55] were not included in the current research since the phase boundaries in the composition range of 33.3-100 at.% Y were determined based on analogy with the phase equilibria in the Al-Mg-(La, Ce, Pr, and Nd) ternary systems.

CHAPTER3

THERMODYNAMIC MODELING

3.1 METHODOLOGY OF THERMODYNAMIC MODELING

Kaufman and Bernstien [56] introduced the CALPHAD (computer calculation of phase diagram) approach to model the complex phase equilibria in multicomponent alloys. This method is based on computational thermodynamics: given the Gibbs energies of all the competing phases in a system, the final equilibrium state at a given composition, temperature and pressure can be calculated by minimizing the total Gibbs energy of the system:

$$\text{minimize} \quad G = \sum_P n_P G_P \tag{3.1}$$

where n_p is the number of moles of phase p and G_p is its Gibbs energy.

The CALPHAD method showed a great success in calculating multicomponent phase diagrams for technological applications. However, Chang *et al.* [3] pointed out some shortcomings of some software which were based on the CALPHAD route in calculating the phase diagram. These shortcomings are: (a) the inability of first generation software such as ThermoCalc [57], FactSage [58], and other software to calculate the stable phase diagram of a system from a given thermodynamic description

especially when the Gibbs energy function is a multiple minima function and (b) the use of some inappropriate thermodynamic models especially for ordered phases.

For these reasons, a second generation software, PANDAT package [4], has been used in this work for thermodynamic modeling and optimization. PANDAT software was developed based on global optimization algorithms and always calculates the stable phase diagrams for a given set of thermodynamic parameters, and no initial guesses are needed to be provided. In contrast, according to Chang *et al.* [3], the first generation software are based on the local minimization technique which does not guarantee the calculation of the stable phase diagram. The methodology of this work is illustrated in the flow chart shown in Figure 3.1.

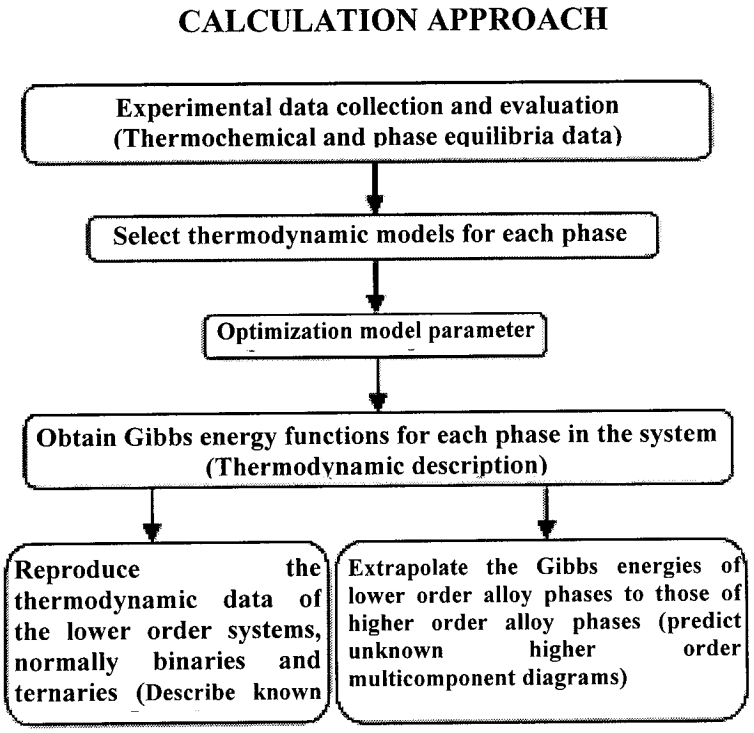

***Figure 3.1**: the CALPHAD phenomenological approach used to obtain the thermodynamic description of a multicomponent system [3]*

As mentioned earlier the first step of the thermodynamic modeling is collecting the experimental data from the relevant literature. The second step is the critical evaluation of these data as discussed in Chapter 2. The third step is selecting suitable thermodynamic model for each phase. The selected model should represent the *P-T-x* domain, in which the phase is stable, further the model should have reasonable extrapolation characteristics in the higher order systems [16]. The fourth step is the optimization the process using the experimental data. The fifth stage is using the calculated Gibbs energy models to reproduce the phase diagram and the thermodynamic data, to verify the agreement between the calculations and the experimental data from the literature. The forth and fifth steps are iterative steps until a good agreement with the experimental data is achieved. The sixth step is the extrapolation to higher order systems from lower ones. In PANDAT package the extrapolation geometry technique is based on Muggianu model [3] which will be explained later in this chapter.

3.2 ANALYTICAL DESCRIPTION OF THE EMPLOYED THERMODYNAMIC MODELS

3.2.1 Unary Phases

The Gibbs Energy function ${}^{0}G_i^{\phi}(T) = G_i^{\phi}(T) - H_i^{SER}$ used for the pure elements i (i = Al, Mg, and Y) in the phase ϕ is described by the following equation:

$${}^{0}G_i^{\phi}(T) = a + bT + cT\ln T + dT^2 + eT^3 + fT^{-1} + gT^7 + hT^{-9} \qquad (3.2)$$

where ${}^0G_i^{\phi}(T)$ represents the Gibbs energy of the pure element, $G_i^{\phi}(T)$ is the Gibbs energy of the pure element at standard state, H_i^{SER} (the molar enthalpy of the stable element reference (SER)) is at 25°C and 1atm, and T is the absolute temperature. The values of the coefficients *a* to *h* are taken from the SGTE (Scientific Group Thermodata Europe) compilation of Dinsdale [60].

3.2.2 Stoichiometric phases

The Gibbs energy of binary stoichiometric phases is given by

$$G^{\phi} = x_i {}^0G_i^{\phi_1} + x_j {}^0G_j^{\phi_2} + \Delta G_f \qquad (3.3)$$

where x_i and x_j are mole fractions of elements i and j and are given by the stoichiometry of the compound, ${}^0G_i^{\phi_1}$ and ${}^0G_j^{\phi_2}$ are the respective reference states of elements i and j, and ΔG_f is the Gibbs energy of formation per mole of atoms of the stoichiometric compound, which is expressed by the following equation:

$$\Delta G_f = a + b.T \qquad (3.4)$$

The parameters *a* and *b* are obtained by optimization using experimental results of phase equilibria and thermodynamic data.

3.2.3 Disordered solution phases

The Gibbs energy of a disordered solution phase is described by the following equation:

$$G^{\phi} = x_i {}^0G_i^{\phi} + x_j {}^0G_j^{\phi} + RT[x_i \ln x_i + x_j \ln x_j] + {}^{ex}G^{\phi} \qquad (3.5)$$

where ϕ denotes the phase of interest and x_i, x_j denote the mole fraction of component i and j, respectively. The first two terms on the right hand side of equation 3.5 represent the Gibbs energy of the mechanical mixture of the components, the third term is the ideal Gibbs energy of mixing, and the fourth term is the excess Gibbs energy, which is described by the Redlich-Kister polynomial model [61] in this work and can be represented as:

$$^{ex}G^{\phi} = x_i.x_j \sum_{n=0}^{n=m} {}^{n}L_{i,j}^{\phi}(x_i - x_j)^n \tag{3.6}$$

$$^{n}L_{i,j}^{\phi} = a_n + b_n \times T \tag{3.7}$$

where a_n and b_n are the model parameters to be optimized with the experimental phase diagram and thermodynamic data.

3.2.4 Solid solution phases

The Gibbs energy of an ordered solution phase is described by the compound energy formalism as shown in the following equations:

$$G = G^{ref} + G^{ideal} + G^{excess} \tag{3.8}$$

$$G^{ref} = \sum y_i^l y_j^m \ldots . y_k^q {}^{0}G_{(i:j:\ldots:k)} \tag{3.9}$$

$$G^{ideal} = RT \sum_l f_l \sum_i y_i^l \ln y_i^l \tag{3.10}$$

$$G^{excess} = \sum y_i^l y_j^l y_k^m \sum_{\gamma=0} {}^{\gamma}L_{(i,j):k} \times (y_i^l - y_j^l)^{\gamma} \tag{3.11}$$

where $i, j, \ldots k$ represent components or vacancy, l, m and q represent sublattices. y_i^l is the site fraction of component i on sublattice l. f_l is the fraction of sublattice l relative to the

total lattice sites. ${}^{0}G_{(i:j:..k)}$ represents a real or a hypothetical compound energy. ${}^{\gamma}L_{(i,j)}$ represent the interaction parameters which describe the interaction within the sublattice.

3.3 Extrapolation Technique

The Muggianu model [59] is one of the models by which the ternary phase diagram and the thermodynamic properties of the ternary system are extrapolated using the three constitutive binary systems. PANDAT software [4] uses this model for extrapolation.

This model is classified as a symmetrical model by Hillert [62]. The graphical interpretation of this model is shown in Figure 3.2.

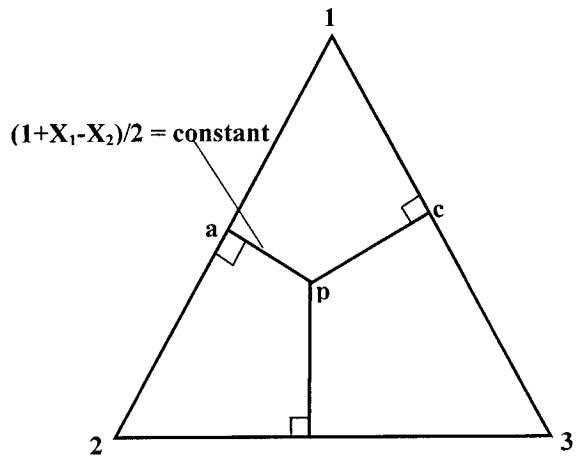

Figure 3.2: *Geometrical interpretation of the Muggianu model [63].*

The excess Gibbs energy in the ternary solution at composition p is described from the excess Gibbs energies of the three binaries at point a, b, and c using the Redlich-Kister form by the following equation [63].

$$g_P^E = x_1.x_2\alpha_{12(a)} + x_2.x_3\alpha_{23(b)} + x_1.x_3\alpha_{13(c)} + (ternary\ terms) \qquad (3.12)$$

where $\alpha_{12(a)}$, $\alpha_{23(b)}$, and $\alpha_{13(c)}$ are the binary excess energy functions evaluated at point a, b, and c. The "ternary terms" are the polynomial terms which are identically zero in the three binary sub-systems. The empirical coefficients of these ternary terms are chosen in order to fit the ternary experimental data [63]. Since the Redlich-Kister formalism is used in PANDAT software [4], then:

$$\alpha_{12} = \sum_{i\geq 0} {}^{i}L_{12}(x_1 - x_2)^i \qquad (3.13)$$

where ${}^{i}L_{12}$ is the empirical coefficients which are represented in equation 3.7.

along the line *ap* in Figure 3.2, the ratio $\frac{1 + X_1 - X_2}{2} =$ constant.

at point "*a*" in the binary 12, and according the binary phase diagram rules

$$X_1 + X_2 = 1 \qquad (3.14)$$

then,

$$X_1 = \frac{1 + X_1 - X_2}{2} \qquad (3.15)$$

by substituting equations; 3.15, 3.14, and 3.13 in 3.12 the resulting formula is identified as the Muggianu model [59] as represented by the following equation:

$$\Delta G^{E} = \frac{4x_1x_2}{(1+x_1-x_2)(1+x_2-x_1)}\Delta G^{E}_{12}\left(\frac{1+x_1-x_2}{2};\frac{1+x_2-x_1}{2}\right)+$$
$$+\frac{4x_2x_3}{(1+x_2-x_3)(1+x_3-x_2)}\Delta G^{E}_{23}\left(\frac{1+x_2-x_3}{2};\frac{1+x_3-x_2}{2}\right)+$$
$$+\frac{4x_3x_1}{(1+x_3-x_1)(1+x_1-x_3)}\Delta G^{E}_{31}\left(\frac{1+x_3-x_1}{2};\frac{1+x_1-x_3}{2}\right)+$$
$$+(\textit{ternary term}) \qquad (3.16)$$

where ΔG^{E} and $\Delta G^{E}ij$ correspond to the integral molar excess Gibbs energy for ternary and binary systems, respectively, where x_1, x_2, x_3 point to the mole fraction of components.

CHAPTER4

RESULTS AND DISCUSSION OF Al-Y AND Mg-Y BINARY SYSTEMS

4.1 OPTIMIZATION OF Al-Y SYSTEM AND CALCULATION OF ITS THERMODYNAMIC PROPERTIES

4.1.1 Al-Y Phase Diagram

In 1989, Ran *et al.* [62] calculated the Al-Y system for the first time. They used 5-Redlich-Kister polynomial terms for the liquid phase, however, their results did not show an agreement with the experimental results of the integral heat of mixing and partial activities. In 1995, Gröbner *et al.* [33] reoptimized the system with 5- Redlich-Kister polynomial terms for the liquid phase in order for to be it used in the extrapolation of Al-Y-C ternary system. In their work, the AlY compound was considered as a congruent melting compound, this disagrees with the experimental data obtained by [18,19,23]. Also, their model does not reproduce the experimental thermodynamic data reported in the literature except for the heats of formation of the intermetallic compounds.

The selected experimental phase diagram and enthalpy of mixing of liquid Al-Y alloys, which were discussed in Section 2.1, were used to optimize the thermodynamic model parameters for all the phases in the Al-Y binary system. In order to maintain the

consistency with other systems modeled by our group, and by the COST507 project [15], no lattice stability values are added to the Gibbs energy expressions obtained from the SGTE database [60] for the pure components; Fcc-Al, Hcp-Y, and Bcc-Y.

In the current work the Al-Y system was reoptimized and calculated using 3-Redlich-Kister terms for the liquid as shown in Table 4.1. In general, a simpler model with fewer number of parameters is preferred to the more complicated one.

Table 4.1: *The optimized model parameters for the liquid and intermetallic compounds in the Al-Y system.*

Phase	Terms	a(J/mole atom)	b(J/mol)
Liquid	L_0	-160 876.360	50
	L_1	-32 000	7.56
	L_2	32 000	-6.53
Al_3Y	ΔG_f	-39 727.972	8.036
Al_2Y	ΔG_f	-50 410.046	10.230
AlY	ΔG_f	-48 074.303	11.536
Al_2Y_3	ΔG_f	-45 347.395	12.364
AlY_2	ΔG_f	-38 200	10.568

The model-calculated phase diagram of the Al-Y system in relation to the experimental results from the literature is shown in Figure 4.1. This figure shows a good agreement with the published experimental data.

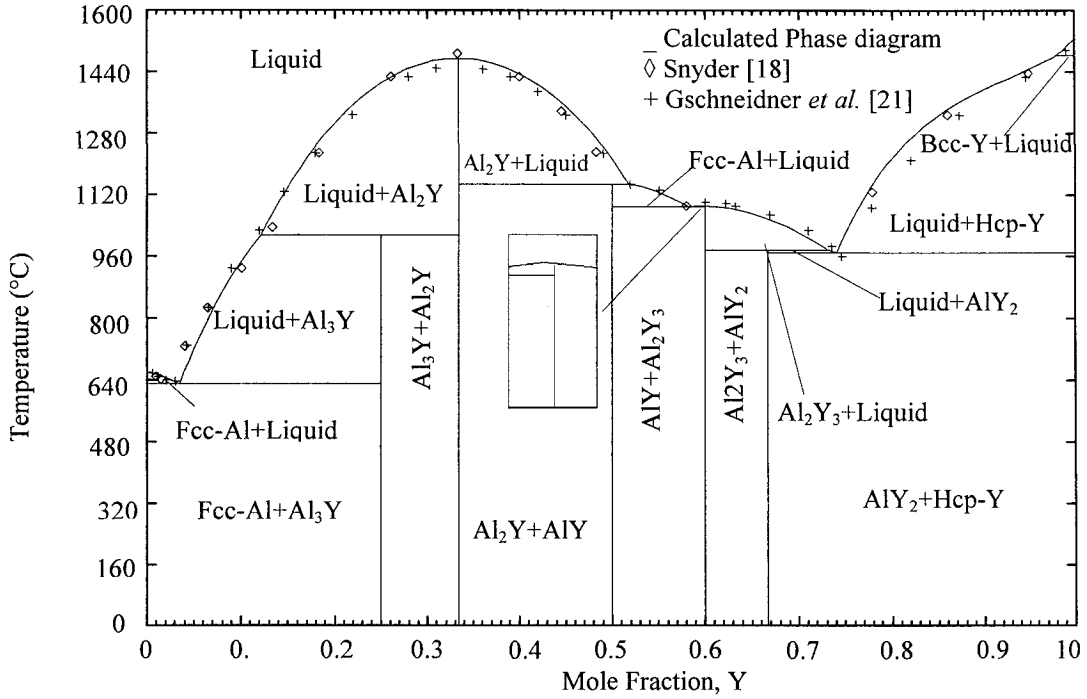

Figure 4.1: *Calculated Al-Y phase diagram with experimental results from the literature.*

A comparison between the current results and other work on this system is shown in Table 4.2.

Table 4.2*: Comparison between the calculated model for Al-Y phase diagram work and other work.*

Reaction	**Temp. (°C)**	**Comp. (X_Y%)**	*Reference*
Liquid⇆Fcc-Al+Al_3Y	636	2.7	This work
	638.7	1.8	[64]
	640	2.1	[33]
Liquid ⇆AlY+Al_2Y_3	1085.4	57	This work
	1092.2	57.19	[64]
	1078	58	[33]

Liquid ⇆AlY_2+Hcp-Y	967.3	74	This work
	964	76.88	[64]
	962	73	[33]
Liquid + Al_2Y ⇆Al_3Y	984	25	This work
	981.5	25	[64]
	980	25	[33]
Liquid ⇆Al_2Y	1478	33	This work
	1447	33	[64]
	1485	33	[33]
Liquid + Al_2Y ⇆AlY	1130	50	This work
	1130	50	[64]
	1130*	50	[33]
Liquid ⇆Al_2Y_3	1091	60	This work
	1089	60	[64]
	1100	60	[33]
Liquid + Al_2Y_3 ⇆AlY_2	978	67	This work
	980	67	[64]
	985	67	[33]
Hcp-Y ⇆ Bcc-Y, Liquid	1478.4	1.0	This work
	1477	97.88	[64]
	1479	98.7	[33]

* ***considered as congruent compound***

4.1.2 Thermodynamic Data

The calculated heat of mixing, shown in Figure 4.2, illustrates a good agreement with the experimental data obtained by [29,30], except in the 0.33-0.55 composition range where the experimental data shows a negative deviation over the calculated one, however, both of them have the minimum point at the same composition. This deviation is not only between the calculated and the experimental data; it can be also seen between the experimental results of Ryss *et al.* [29] and Esin *et al.* [30] as shown in Figure 4.2. This

discrepancy is probably due to the difficulty in obtaining accurate measurements in this region, because of the existence of the high melting Al_2Y compound (T_m = 1475°C). However, the work of Petrov *et al.* [32] shows a large discrepancy with the current calculation as well as with the work of [29] and [30]. This discrepancy is probably due to the less accurate vapor pressure experimental technique used by [32] than the calorimetric experimental technique which was used by [29,30].

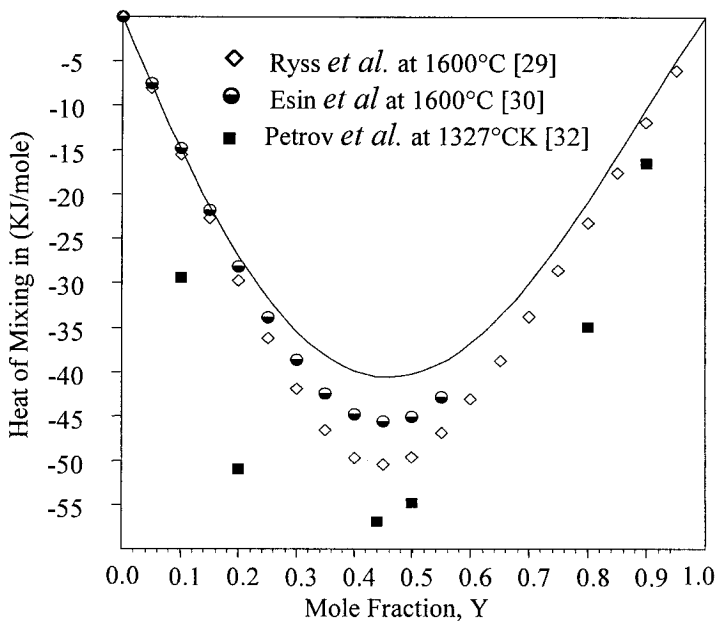

Figure 4.2 Calculated heat of mixing of the Al-Y system at 1600°C compared with experimental data from the literature.

The calculated activities are shown in Figure 4.3 where a good agreement with Petrusheveskii and Ryss [36] can be observed. However, the activity measured by Kulfieev *et al.* [37] shows poor agreement with the calculated data. This is due to the

systematic error, which is attributed to using different techniques in activity measurement [6].

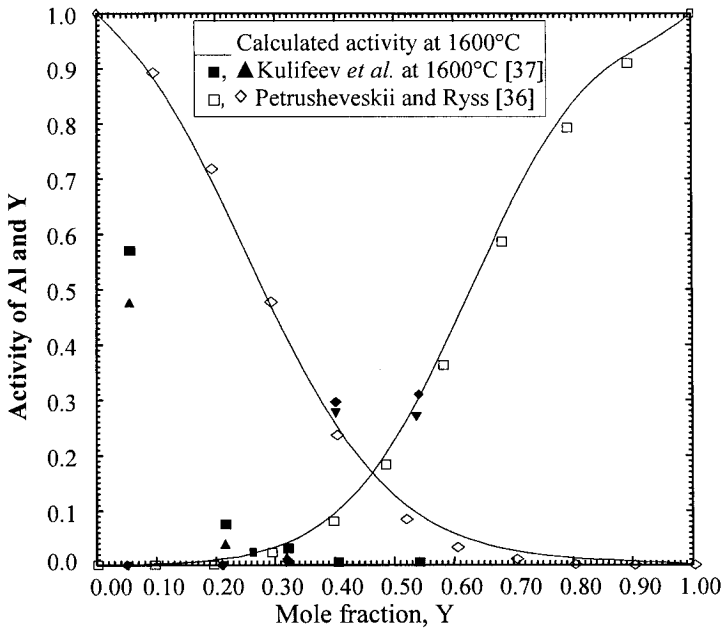

Figure 4.3: *Calculated activities of Al and Y at 1600°C with experimental data from the literature.*

The calculated partial heats of mixing of Al and Y show a good agreement with the experimental data obtained by [29,30] as shown in Figure 4.4. A slight positive deviation is noticed in the calculated data over the experimental one. Nonetheless, the trend is similar. However, the experimental partial heats of mixing of Al and Y which were obtained by Petrov *et al.* [32] show a poorer agreement with the calculated partial heat of mixing and contradict the experimental work of [29] and [30]. This contradiction is, again, due to the difference in the experimental techniques used in these studies.

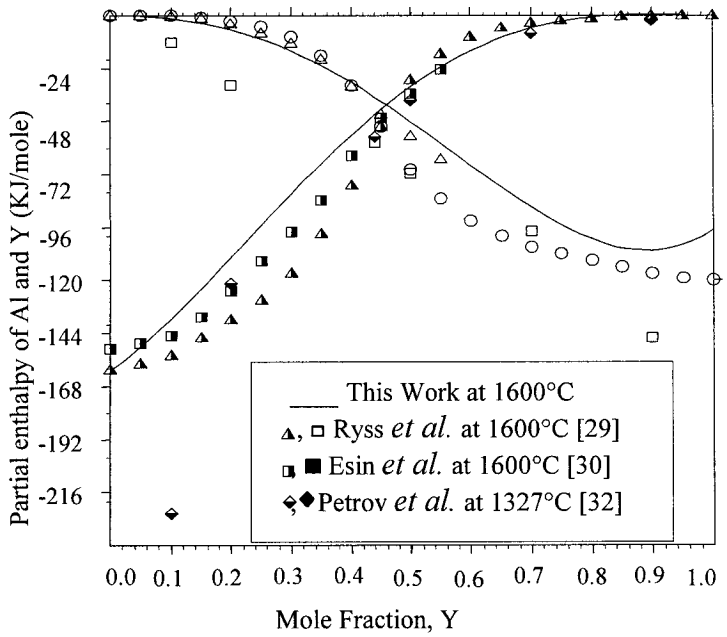

Figure 4.4: *Calculated partial heat of mixing of Al and Y in the Al-Y liquid at 1600°C compared with experimental data from the literature.*

Figure 4.5 shows a good agreement between the calculated heats of formation obtained in this study and the experimental results reported by [33,35]. On the other hand, the heats of formation of Al_2Y, Al_3Y, and AlY which were measured by Snyder [18] are more negative than the calculated ones. This higher negativity is caused by employing the Miedema *et al.* [65] estimations to calculate the heat of formations of the three intermetallic compounds. The calculated heat of formation of the most stable intermetallic compound Al_2Y shows an excellent agreement with the results of [27,33] as shown in Figure 4.5.

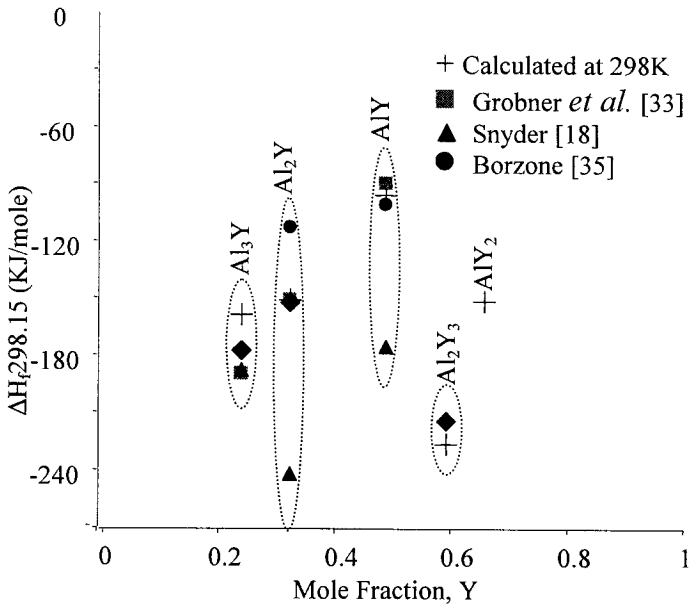

(d)

Figure 4.5 *Calculated heat of formations of the intermetallic compounds in Al-Y binary system at 25°C compared with experimental data from the literature.*

4.2 OPTIMIZATION OF THE Mg-Y SYSTEM AND CALCULATION OF ITS THERMODYNAMIC PROPERTIES

4.2.1 Mg-Y phase diagram

In 1988, Ran *et al.* [49] calculated the Mg-Y phase diagram using the optimized parameters of phase equilibria and thermodynamic data. In their work, δ-phase was considered stoichiometric. However, Flandorfer *et al.* [43] had reported a range of homogeneity for this compound. The assessment of the thermodynamic data from the related literature such as the heat of mixing, activities and partial Gibes free energy was not discussed by Ran *et al.* [49].

In 2003, Fabrichanya *et al.* [46] recalculated the Mg-Y system using both the phase equilibria and thermodynamic data in the optimization process. They used the sublattice model and they reproduced the homogeneity ranges of ε, δ, and γ^{Mg-Y}. Their calculations showed a good agreement with the phase diagram and the thermodynamic data from the related literature. Although they reproduced the homogeneity ranges of ε, δ, and γ^{Mg-Y} phases in their calculation, they did not consider the crystallographic data for ε, δ, and γ^{Mg-Y} phases in the modeling process. Besides, they modeled the γ^{Mg-Y} phase using at least 10 parameters which can result in unpredictable calculations for the higher order systems [16]. Therefore, this system will be reoptimized during the course of this research.

In the current work, the Mg-Y system was reoptimized using the experimental data of the phase equilibria by employing the Redlich-Kister model for the liquid, Hcp-

Mg, and β-Y phases, and the general compound energy formalism (CEF) or sublattice model for the ε, δ, and γ^{Mg-Y} phases as shown in Table 4.3.

***Table 4.3**: Optimized Redlich-Kister model parameters for all the phases in Mg-Y system.*

Phase	Terms	a (J.mole^{-1} atom)	b (J.mole^{-1}K)
Liquid	L_0	-40 917.97	22.83
	L_1	-18 685.23	10.24
	L_2	1 076.67	-6.05
Hcp-Mg	L_0	- 11 718.26	7.49
	L_1	-4 305.6	2.43
	L_2	-7 236.36	2
β-Y	L_0	-28 199.32	13.49
	L_1	-2 005	1.5
Phase	**Terms**	**a (J.mole^{-1} per formula unit)**	**b (J.mole^{-1}K)**
ε, $Mg_{24}Y_5$	G (Mg: Mg: Mg)	1 419	0
	G(Mg: Y: Mg)	-6 050	0
	G(Y: Y: Mg)	6 000	-3
δ, Mg_2Y	G(Mg: Mg: Mg)	1 800	0
γ^{Mg-Y}	G(Mg: Y: Mg)	-8 870	-0.05
	G(Y: Y: Mg)	4 000	0
	G(Y: Mg: Mg)	-5 000	163.02
	L (Mg, Y: Mg: Mg; 0)	-5 000	336.16
	L (Mg, Y: Y: Mg; 0)	-7 816.92	20.44
	L (Mg: Mg, Y: Mg; 0)	-3 910.068	3.47
	L (Y: Mg, Y: Mg; 0)	-5 000	336.44
	G(Mg: Y)	-19 350	1.21
	G(Mg:Va)	10 000	0.0
	G(Y:Y)	-5 791.56	21.5
	G(Y:Va)	27 000	35
	L (Mg,Y: Y;0)	15 000	16
	L (Mg, Y: Va; 0)	15 000	15
	L (Mg: Y, Va; 0)	-5 000	7
	L (Y: Y, Va; 0)	-5 000	7

The calculated phase diagram shows a good agreement with the experimental data from the literature as shown in Figure 4.6. The calculated ranges of homogeneities are also consistent with experimental data as shown in Figure 4.6.

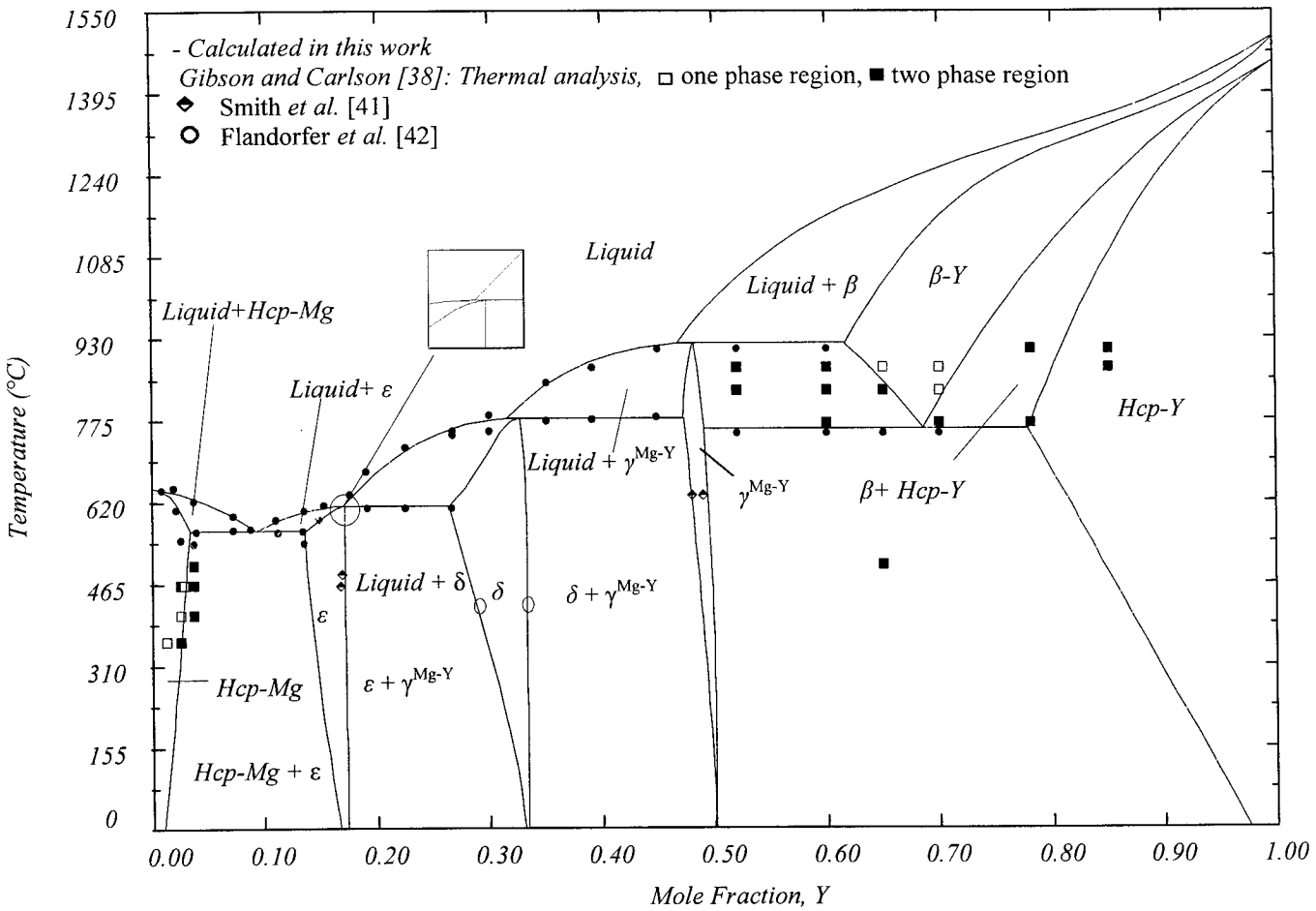

Figure 4.6: *Calculated Mg-Y phase diagram with experimental results from the literature.*

A comparison between the results of this work and the recent calculations of the Mg-Y systems is presented in the Table 4.4.

Table 4.4*: Comparison the Calculated Mg-Y phase diagram and other works.*

Reaction	**Temp. (°C)**	**Comp. (X_Y%)**	**Solution Model**	*Reference*
Liquid ⇆Hcp-(Mg or Y, be specific)+ε	566	7.85	Redlich-Kister polynomial	This work
	567	8.14	Redlich-Kister polynomial	[49]
	572	8.2	Subistituational model	[46]
B-Y ⇆ Hcp-Y + γ^{Mg-Y}	773	69	Redlich-Kister polynomial	This work
	775	72	Redlich-Kister polynomial	[49]
	777	69	Redlich-Kister polynomial	[46]

Liquid + $\gamma^{Mg-Y} \leftrightarrows \delta$	780	30.2	Sublattice model	This work
	782*	25.87	Stoichiometric model	[49]
	783	28.9	Sublattice model	[46]
Liquid + $\delta \leftrightarrows \varepsilon$	625	16.7	Sublattice model	This work
	625	14.36	Wagner Schottky	[49]
	608	14.1	Sublattice model	[46]
Liquid+ β-Y $\leftrightarrows \gamma^{Mg-Y}$	936	47.7	Sublattice model	This work
	934	41.4	Wagner Schottky	[49]
	942	47.2	Sublattice model	[46]

considered as a linear compound

From Table 4.4, it is noticed that there are some discrepancies between this work and the work of Ran *et al.* [49], especially at the compositions where δ, and γ^{Mg-Y} decompose. This is because, δ-phase was considered as a linear compound by Ran *et al.* [49]. However, a good agreement has been achieved between this work and Fabrichanya *et al.* [46] as shown in Table 4.4.

4.2.2 Thermodynamic modeling of the ε, δ, and γ^{Mg-Y} phases

As first approximation of the Mg-Y system, the ε, δ, and γ^{Mg-Y} phases were modeled as linear compounds using the stoichiometric model. Once a satisfactory thermodynamic description of each phase, especially the liquid phase, was obtained, these phases were remodeled as solid solutions using the sublattice model. This was done gradually starting with the highest melting temperature γ^{Mg-Y} phase and ending with the lowest melting temperature ε-phase. This is because the highest melting temperature compound has more effect on the thermodynamic description of the other phases.

Hari Kumar *et al.* [66] and Hari Kumar and Wollants [16] mentioned that attention should be given to the crystallographic information and the solubility range of the phase during the optimization of the sublattice model parameters. The mixing characteristics are commensurate with the data on the range of homogeneity and the crystallographic information is mainly required for deciding the number of sublattices to be used and for assigning constituents species to each of them.

4.2.2.1 Thermodynamic modeling of the γ^{Mg-Y} phase

The crystal structure data of the γ^{Mg-Y} intermediate solid solutions is obtained by Smith *et al.* [42] and listed in the Pearson handbook [67] as shown in Table 4.5.

Table 4.5: *Crystal structure and lattice parameters of γ^{Mg-Y} phase.*

Phase	Crystal data		Atoms	WP[1]	CN[2]	PS[3]	Atomic position			Ref.
							X	Y	Z	
γ^{Mg-Y}, MgY	Structure Type	ClCs	Mg	1a	14	*m-3m*	0	0	0	[67]
	Pearson Symbol	*CP2*	Y	1b	14	*m-3m*	½	½	½	
	Space Group	*P m-3m*								
	Space Group No.	221								
	Lattice parameter (nm)	A=0.3810								
	Angles: α= 90, β=90, γ=120									

[1]***WP= Wyckoff Position,*** [2]***CN=Coordination Number and*** [3]***PS=Point Symmetry***

The coordination numbers which are shown in Table 4.5 are obtained in this work. The coordination number is defined as the number of closest neighbor similar and dissimilar atoms around the atom of interest [66]. This number is determined from the substructure of each atom which was drawn by the PowderCell software [68] using the available crystallographic data as shown in Figure 4.7.

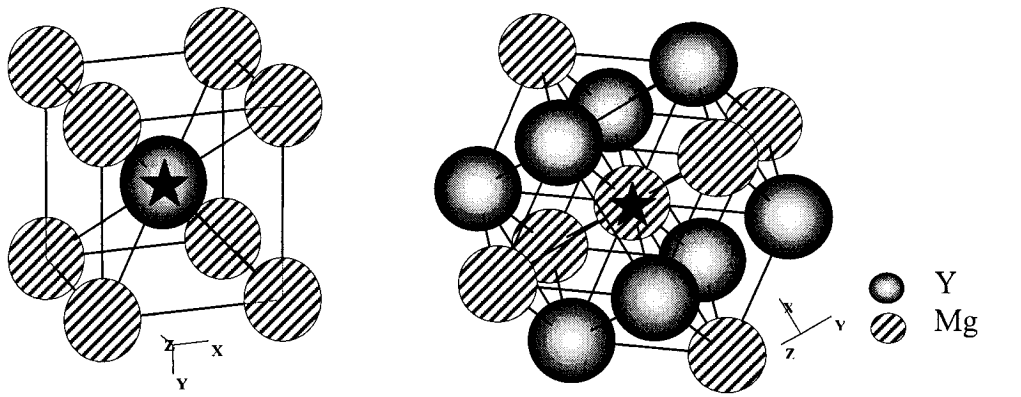

Figure 4.7: *Substructure of (a) Y and (b) Mg atoms in γ^{Mg-Y} unit cell with the coordination number (CN).*

Based on crystallographic data of γ^{Mg-Y} phase, there are two atoms at different sites in the unit cell with the same point of symmetry and different coordination number as shown in Table 4.5. To obtain an intermediate phase which has an ideal stoichiometry, two sublattices are needed and each sublattice is occupied by only one constituent species. In other words the direct sublattice model which is composed based on the crystallographic data of γ^{Mg-Y} phase only is the following model:

$$(Mg)_1 : (Y)_1$$

This model does not represent the homogeneity range of γ-phase which was obtained by Smith *et al.* [41]. To achieve the deviation from stoichiometry, it is necessary to allow mixing of atoms in one or more sublattices. For the phases which have relatively a narrow range of homogeneity like γ^{Mg-Y} the mixing is performed by "defects", which

may be vacancies or antistructure atoms (i.e. atoms at lattice sites belonging to the other kind of atoms in the ideal structure) [16,66]. Based on that, the mixing of Y atoms as antistructure atoms in Mg sublattice and vacancies (Va) in Y sublattice are the defects considered in this model. Therefore, the model takes the form:

$$(Mg\%, Y)_1 : (Y\%: Va)_1$$

Here the '%' denotes the major constituent of the sublattice. The range which is covered by this model is the whole composition range. Therefore, this satisfies the homogeneity range requirement for $\gamma^{Mg\text{-}Y}$ phase which was obtained by Smith *et al.* [42] as $0.48 \leq X_Y \leq 0.5$.

Hence, the Gibbs energy per mole of formula unit of MgY is given by the following equation.

$$\begin{aligned} G_m^{MgY} &= y_{Mg}^I y_Y^{II}\,{}^0G_{Mg:Y}^{MgY} + y_{Mg}^I y_{Va}^{II}\,{}^0G_{Mg:Va}^{MgY} + y_Y^I y_Y^{II}\,{}^0G_{Y:Y}^{MgY} + y_Y^I y_{Va}^{II}\,{}^0G_{Y:Va}^{MgY} \\ &+ RT\left(0.5\sum_{i=Mg}^{Y} y_i^I \ln y_i^I + 0.5\sum_{i=Y}^{Va} y_i^{II} \ln y_i^{II}\right) + y_{Mg}^I y_Y^I \left(y_Y^{II}\,{}^0L_{Mg,Y:Y}^{MgY} + y_{Va}^{II}\,{}^0L_{Mg,Y:Va}^{MgY}\right) \\ &+ y_Y^{II} y_{Va}^{II}\left(y_{Mg}^I\,{}^0L_{Mg:Y,Va}^{MgY} + y_Y^I\,{}^0L_{Y:Y,Va}^{MgY}\right) \end{aligned} \tag{4.1}$$

where, I is the species inside the sublattice.

y_{Mg}^I, y_Y^I is the site fraction of sublattice I.

y_Y^{II}, y_{Va}^{II} is the site fractions of lattice II.

$^{0}G^{MgY}_{Mg:Y}$, $^{0}G^{MgY}_{Mg:Va}$, $^{0}G^{MgY}_{Y:Y}$, $^{0}G^{MgY}_{Y:Va}$, $^{0}L^{MgY}_{Mg,Y:Y}$, $^{0}L^{MgY}_{Mg,Y:Va}$, $^{0}L^{MgY}_{Mg:Y,Va}$, *and* $^{0}L^{MgY}_{Y:Y,Va}$ are the parameters that were optimized by employing the CEF with the experimental data shown in Table 4.3 using PANDAT package [4].

4.2.2.2 Thermodynamic modeling of the ε-phase

The crystallographic data of ε-phase were provided recently by Zhank and Kelly *et al.* [44] and are presented in Table 4.6.

Table 4.6: *Crystal structure and lattice parameters of ε -phase.*

Phase	Crystal data		Atoms	WP[1]	CN[2]	PS[3]	Atomic position			Ref.
							X	Y	Z	
ε, $Mg_{24}Y_5$	Structure Type	Mn	Y1	2a	16	*m43-*	0	0	0	[44]
	Pearson Symbol	*CI58*	Y2	8c	16	3m	0.3126	0.3126	0.3126	
	Space Group	*I-43m*	Mg1	24g	12	m	0.3605	0.3605	0.3605	
	Space Group No.	217	Mg2	24g	12	m	0.0857	0.0857	0.2805	
	Lattice parameter (nm)	a=1.124								
	Angles: α= 90, β=90, γ=90									

[1]WP= Wyckoff Position, [2]CN=Coordination Number and [3]PS=Point Symmetry

The coordination number of each atom in the crystal was determined from the substructure of each atom in this phase as shown in Figure 4.8.

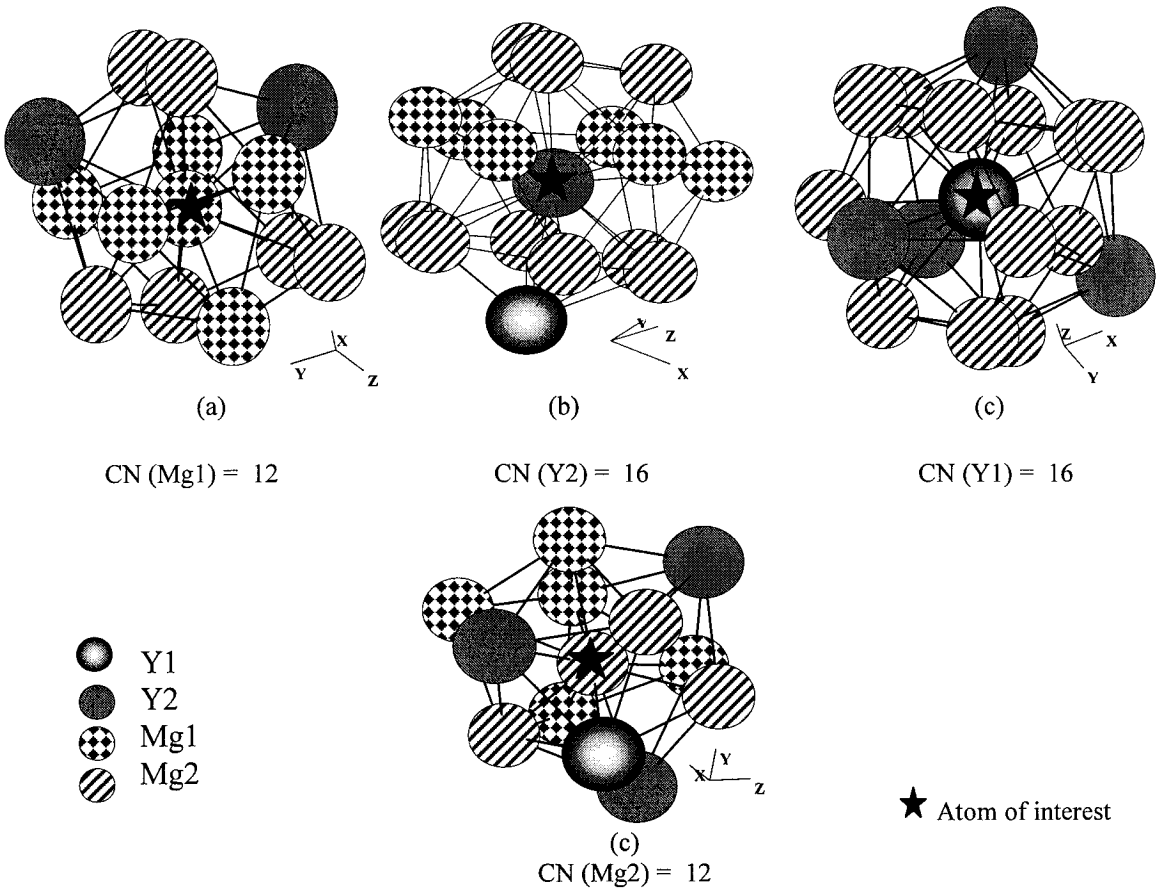

Figure 4.8: *Substructure of (a) Mg1, (b)Y2, (c) Y1, and (d) Mg2 atoms in ε unit cell with the CN.*

The crystallographic data indicate that the unit cell of the ε-phase has 58 atomic positions; 2 for Y1, 8 for Y2, 24 for Mg1, and 24 for Mg2. Hence, the direct sublattice model based on the crystallographic data is:

$$(Mg1)_{24} :(Mg2)_{24} :(Y1)_2 :(Y2)_8$$

This model represents the $Mg_{48}Y_{10}$ stoichiometric compound; however it does not illustrate the homogeneity range of ε-phase. To obtain the homogeneity range from the sublattice model, grouping of sublattices and mixing of species is applied.

According to Kumar and Wollants [49], the sublattices which have the same coordination number and /or the point symmetry can be grouped. Based on that, Mg1 and Mg2 are grouped in one sublattice, on the other hand Y1 and Y2 were also grouped in another sublattice. This results in the following model:

$$(Mg)_{48} :(Y)_{10}$$

Allowing mixing in this model with antistructure atoms in each sublattice will not give us the homogeneity range which was reported by Smith *et al.* [42]. To obtain the homogeneity range, the sublattice which is occupied by Mg atom is divided into two sublattices; the first sublattice with 29 sites and the second sublattice with 19 sites as in the following model:

$$(Mg)_{29} :(Y)_{10}: (Mg)_{19}$$

The mixing of Y and Mg antistructure atoms is applied in the first and second sublattices, respectively. Whereas, the mixing in the third sublattice is not needed, because the homogeneity range is already achieved. The generated model after mixing is:

$$(Mg\%, Y)_{29} :(Y\%, Mg)_{10}: (Mg)_{19}$$

The maximum homogeneity range of $0.13 \leq X_Y \leq 0.16$ at 545°C which was reported by Smith *et al.* [41] is included by the range of this model which covers $0 \leq X_Y \leq 0.672$.

Therefore, the Gibbs energy per mole of formula unit of the ε-phase can be written as:

$$\begin{aligned} G_m^{Mg_{24}Y_5} &= y_{Mg}^I y_Y^{II}\, {}^0G_{Mg:Y:Mg}^{Mg_{24}Y_5} + y_{Mg}^I y_{Mg}^{II}\, {}^0G_{Mg:Mg:Mg}^{Mg_{24}Y_5} + y_Y^I y_Y^{II}\, {}^0G_{Y:Y:Mg}^{Mg_{24}Y_5} + y_Y^I y_{Mg}^{II}\, {}^0G_{Y:Mg:Mg}^{Mg_{24}Y_5} \\ &+ RT(0.5\sum_{i=Mg}^{Y} y_i^I \ln y_i^I + 0.172\sum_{i=Y}^{Mg} y_i^{II} \ln y_i^{II}) + y_{Mg}^I y_Y^I (y_{Mg}^{II}\, {}^0L_{Mg,Y:Y:Mg}^{Mg_{24}Y_5} + y_Y^{II}\, {}^0L_{Mg,Y:Mg:Mg}^{Mg_{24}Y_5}) \quad (4.2) \\ &+ y_{Mg}^{II} y_Y^{II} (y_{Mg}^I\, {}^0L_{Mg:Mg,Y:Mg}^{Mg_{24}Y_5} + y_Y^I\, {}^0L_{Y:Mg,Y:Mg}^{Mg_{24}Y_5}) \end{aligned}$$

and $$0.5\sum_{i=Mg}^{Y} y_i^I \ln y_i^I + 0.172\sum_{i=Y}^{Mg} y_i^{II} \ln y_i^{II} + 0.328 y_{Mg}^{III} = 1 \qquad (4.3)$$

where, i is the species in one sublattice.

y_{Mg}^I, y_Y^I are the site fractions of lattice I.

y_{Mg}^{II}, y_Y^{II} are the site fractions of lattice II.

y_{Mg}^{III} is the site fraction of lattice III.

$${}^0G_{Mg:Y:Mg}^{Mg_{24}Y_5}, {}^0G_{Mg:Mg:Mg}^{Mg_{24}Y_5}, {}^0G_{Y:Y:Mg}^{Mg_{24}Y_5}, {}^0G_{Y:Mg:Mg}^{Mg_{24}Y_5}, {}^0L_{Mg,Y:Y:Mg}^{Mg_{24}Y_5}, {}^0L_{Mg,Y:Mg:Mg}^{Mg_{24}Y_5}, {}^0L_{Mg:Mg,Y:Mg}^{Mg_{24}Y_5}, and\ y_Y^I\, {}^0L_{Y:Mg,Y:Mg}^{Mg_{24}Y_5})$$

are the parameters which were optimized using the experimental data listed in Table 4.3.

4.2.2.3 Thermodynamic modeling of the δ-phase

The crystallographic data for the δ-phase were obtained from the literature and are tabulated in Table 4.7.

Table 4.7: *Crystal structure and lattice parameters of* ***δ*** *-phase.*

Phase	Crystal data		Atoms	WP[1]	CN[2]	PS[3]	Atomic position			Ref.
							X	Y	Z	
δ, Mg_2Y	Structure Type	$MgZn_2$	Mg1	2a	6	*-3m*	0	0	0	[42]
	Pearson Symbol	*Hp12*	Mg2	6h	4	*mm2*	0.8409	0.6818	1/4	
	Space Group	*$P6_3/mmc$*	Y	4f	4	*3m*	1/3	2/3	0.6818	
	Space Group No.	194								
	Lattice parameter (nm)	a=0.6037								

[1]***WP= Wyckoff Position,*** [2]***CN=Coordination Number and*** [3]***PS=Point Symmetry***

The coordination number for each atom in the lattice is quantified as in Figure 4.9.

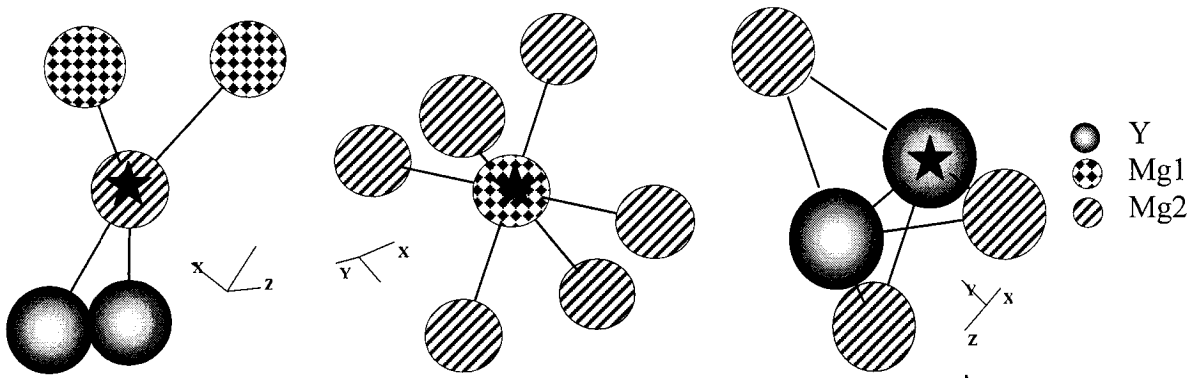

Figure 4.9: : *Substructure of (a) Mg2, (b) Mg1 and (c) Y atoms in* δ *unit cell.*

The direct sublattice model which is derived from the crystallographic data of δ-phase is the following:

$$(Mg1)_2 : (Mg2)_6 : (Y)_4$$

This model represents the stoichiometry of the δ-phase which is the Mg_2Y compound. To obtain a deviation from this stoichiometry, mixing of constituents is applied. Grouping was not allowed in this model, because the coordination number and the point symmetry for each atom is different from the other atoms as shown in Table 4.7

Mixing of Y antistructure atom in the first sublattice and the Mg antistructure atom in the second sublattice is applied. However mixing in the third sublattice is not

needed, since the homogeneity range of δ-phase is achieved by mixing of the constituents in the first two sublattices as follows:

$$(Mg\%, Y)_6: (Y\%, Mg)_4: (Mg)_2$$

This model covers the $0 \leq X_Y \leq 0.833$ composition range. This range includes the homogeneity range of $0.332 \leq X_Y \leq 0.342$ which was reported by Flandorfer *et al.* [43].

Based on this model, the Gibbs energy per mole of formula unit of δ-phase can be written as:

$$G_m^{Mg_2Y} = y_{Mg}^I y_Y^{II} {}^0G_{Mg:Y:Mg}^{Mg_2Y} + y_{Mg}^I y_{Mg}^{II} {}^0G_{Mg:Mg:Mg}^{Mg_2Y} + y_Y^I y_Y^{II} {}^0G_{Y:Y:Mg}^{Mg_2Y} + y_Y^I y_{Mg}^{II} {}^0G_{Y:Mg:Mg}^{Mg_2Y}$$
$$+ RT(0.5\sum_{i=Mg}^{Y} y_i^I \ln y_i^I + 0.33\sum_{i=Y}^{Mg} y_i^{II} \ln y_i^{II}) + y_{Mg}^I y_Y^I (y_{Mg}^{II} {}^0L_{Mg,Y:Y:Mg}^{Mg_2Y} + y_Y^{II} {}^0L_{Mg,Y:Mg:Mg}^{Mg_2Y})$$
$$+ y_{Mg}^{II} y_Y^{II} (y_{Mg}^I {}^0L_{Mg:Mg,Y:Mg}^{Mg_{24}Y_5} + y_Y^I {}^0L_{Y:Mg,Y:Mg}^{Mg_{24}Y_5}) \quad (4.4)$$

$$\text{and, } 0.5\sum_{i=Mg}^{Y} y_i^I \ln y_i^I + 0.33\sum_{i=Y}^{Mg} y_i^{II} \ln y_i^{II} + 0.17 y_{Mg}^{III} = 1 \quad (4.5)$$

Where, i is the lattice species.

y_{Mg}^I, y_Y^I are the site fractions of lattice I.

y_{Mg}^{II}, y_Y^{II} are the site fractions of lattice II.

y_{Mg}^{III} is the site fraction of lattice III .

${}^0G_{Mg:Y:Mg}^{Mg_2Y}, {}^0G_{Mg:Mg:Mg}^{Mg_2Y}, {}^0G_{Y:Y:Mg}^{Mg_2Y}, {}^0G_{Y:Mg:Mg}^{Mg_2Y}, {}^0L_{Mg,Y:Y:Mg}^{Mg_2Y}, {}^0L_{Mg,Y:Mg:Mg}^{Mg_2Y}, {}^0L_{Mg:Mg,Y:Mg}^{Mg_{24}Y_5}, and\ {}^0L_{Y:Mg,Y:Mg}^{Mg_{24}Y_5}$

are the parameters which were optimized using the sublattice model with the experimental data from the literature.

4.2.3 Thermodynamic properties of the Mg-Y system

The calculated heat of mixing shows a good agreement with the experimental results obtained by Agrawal *et al.* [45] as shown in Figure 4.10.

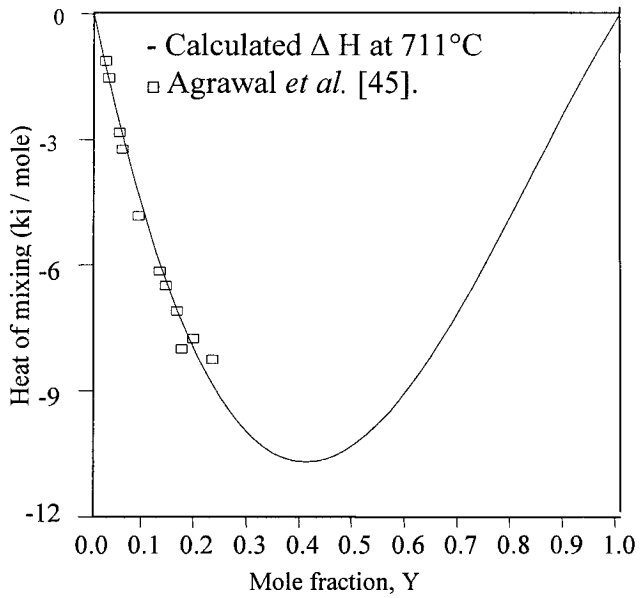

Figure 4.10: *Calculated heat of mixing of the Mg-Y liquid at 711°C in relation to experimental data from the literature.*

The calculated activity of Mg in Mg-Y liquid has a slight negative deviation from the experimental activity which was reported by [44,45] as shown in Figure 4.11. The experimental values of Y activity are not available in the literature therefore comparison was not possible..

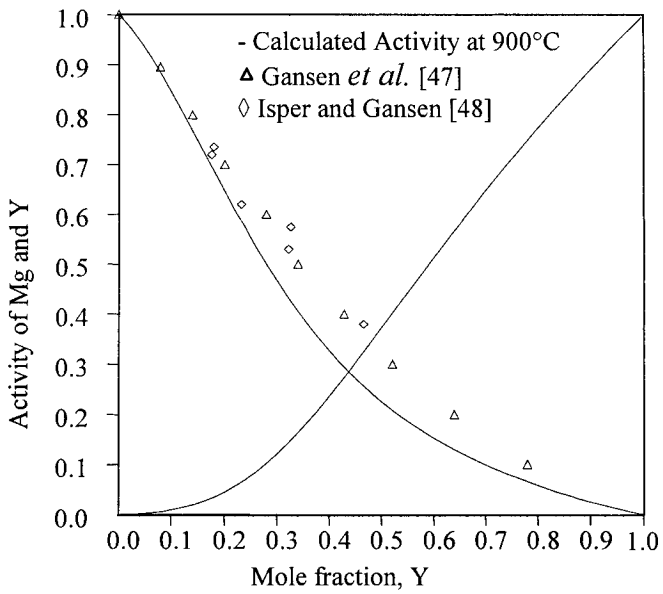

Figure 4.11: *Calculated activities of Mg and Y in Mg-Y liquid at 900°C compared with experimental data for Mg activity from the literature.*

The calculated partial Gibbs free energy of Mg and Y in Mg-Y liquid is in good agreement with the experimental results of [48] as shown in Figure 4.12.

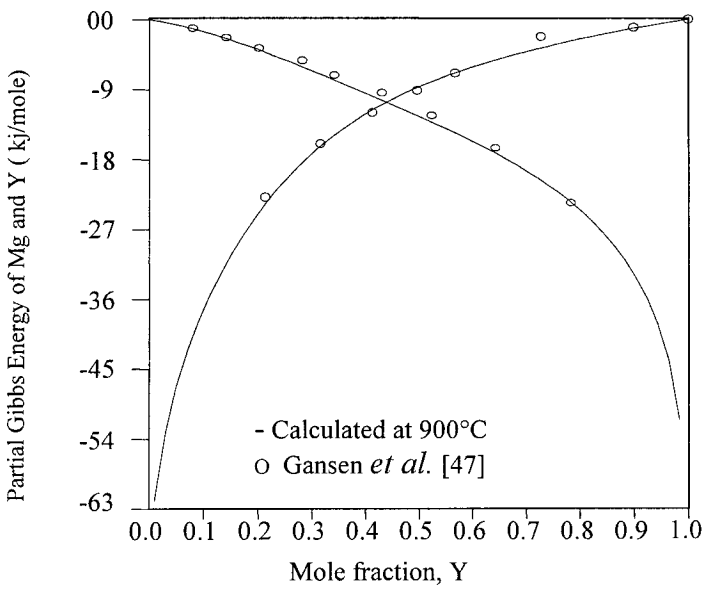

Figure 4.12: *Calculated partial Gibbs energy of Mg and Y in Mg-Y alloy at 900°C compared with experimental data from the literature.*

Figure 4.13 shows the calculated heat of formation of the intermediate compounds in the Mg-Y system in relation to experimental results from the literature. A good agreement between the calculated and the experimental data is noticed. The $\gamma^{Mg\text{-}Y}$ phase, which was reported by [50] has a twice negative value than what was obtained by [42]. and with the value which was calculated in this work. The measurement of Smith *et al.* [42] were more accurate than Pyagai *et al.* [50]. This is because Smith *et al.* [42] used both the calorimetric and vapor pressure techniques which resulted in consistent results. However, Pyagai *et al.* [50] used the calorimetric technique only. The value obtained in the current work lies between these two results but closer to that of Smith *et al.* [42].

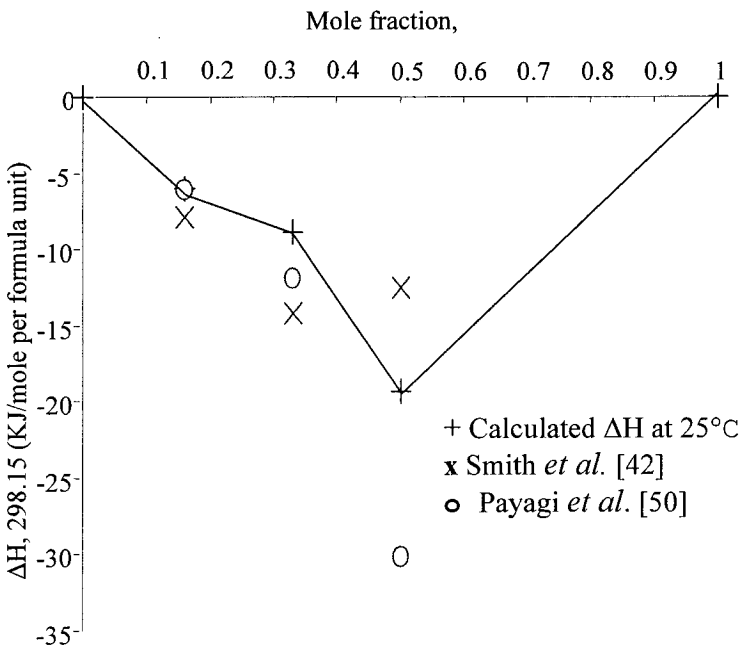

Figure 4.13: *The calculated enthalpies of formation of the stoichiometric compounds compared with experimental data from the literature.*

CHAPTER5

THERMODYNAMIC MODELING OF THE Mg-Al-Y SYSTEM

5.1 Optimization of the Mg-Al-Y system

The main purpose of this work is to construct a self-consistent thermodynamic database for the Mg-Al-Y system. This database has been constructed by combining the thermodynamic descriptions of the three constituent binaries; Al-Y, Mg-Y systems, which were evaluated in this work, and Mg-Al system which was taken from the COST507 database [15], along with the thermodynamic properties of the ternary compound τ (Al_4MgY) which have been assessed in this work.

5.1.1 Thermodynamic modeling of τ-Phase

The ternary compound τ (Al_4MgY) was modeled using the CEF with the experimental data of the primary solidification region which was rported by Odinaev and Ganiev [54]. The values of the parameters of the τ-phase were determined by trial and error using the PANDAT package [4].

The crystal structure of τ-phase was determined by Zarchenyuk *et al.* [53] as shown in the Table 5.1.

Table 5.1: *Crystal structure and lattice parameters of* ***τ*** *–phase.*

Phase	**Crystal data**		**Atoms**	**WP[1]**	**CN[2]**	**PS[3]**	**Atomic position**			**Ref.**
							X	**Y**	**Z**	
τ, Al_4MgY	Structure Type	$MgZn_2$	Al1	2a	12	*-3m*	0	0	0	[53]
	Pearson Symbol	*CP2*	Al2	6h	12	*mm2*	0.83	0.66	0.25	
	Space Group	*P m-3m*	M(Mg,Y)	4f	16	*3m*	1/3	2/	0.062	
	Space Group No.	221								
	Lattice parameter (nm)	a=0.533 c=0.857								
	Angles: α= 90, β=90, γ=120									

[1]WP= Wyckoff Position, [2]CN=Coordination Number and [3]PS=Point Symmetry.

Similarly the coordination number is determined by drawing the substructure of each atom as shown in Figure 5.1.

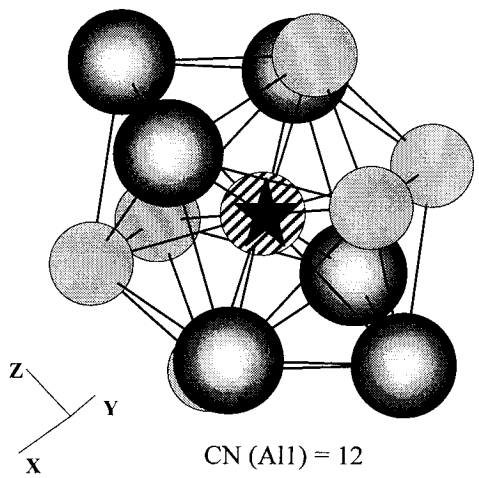

CN (Al1) = 12

(a)

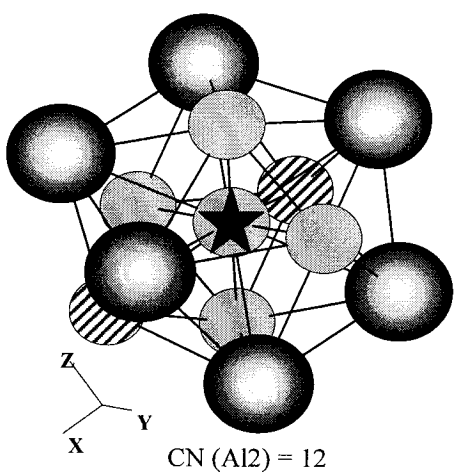

CN (Al2) = 12

(b)

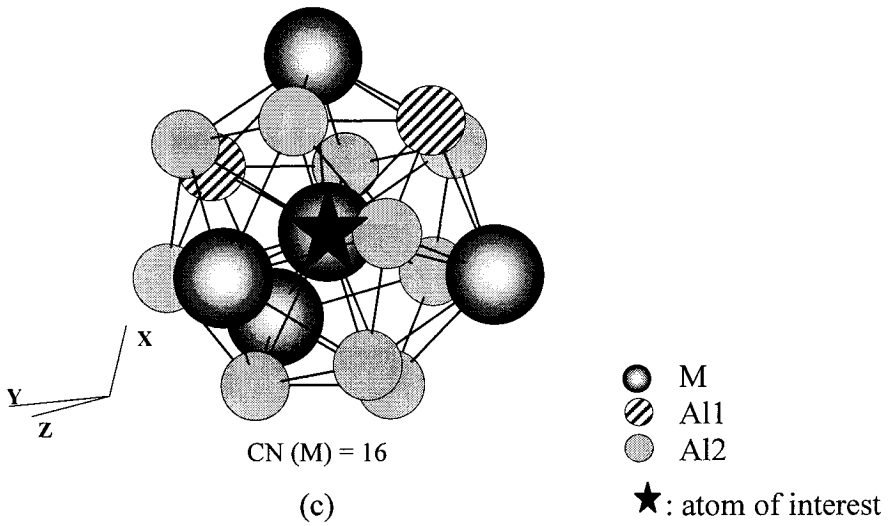

Figure 5.1: *Substructure of (a) M(0.5Mg+0.5Y), (b) Al1 and (c) Al2 atoms in τ-phase unit cell with the CN.*

From the crystal structure of τ-phase, it is noticed that there are three types of atoms at three different positions in the unit cell as shown in Table 5.1. These atoms are; Al1, Al2, and M which represents an atomic site that is occupied by 50 %Mg +50 %Y. Based on the crystallographic data the direct sublattice model is composed as the following:

$$(Al1)_2: (Mg, Y)_4: (Al2)_6.$$

Grouping is allowed between the first and the third lattices, since they have the same coordination number, as the following:

$$(Al)_8: (Mg, Y)_4$$

This model represents the stoichiometric compound Al_4Mg or Al_4Y; however allowing mixing in this model does not give the primary solidification region which was reported by [54]. Hence, another model is proposed, which is also consistent with the

crystallographic understanding of τ-phase. This can be achieved by dividing the (Mg, Y) lattice into three sublattices as the following:

$$(Al)_8: (Mg, Y)_1: (Mg, Y)_{1.6}: (Mg, Y)_{1.4}$$

Mixing is allowed for the second and third sublattice with the antistructure atom Al, and for the first lattice with the antistructure atoms Mg, and Y.; however no mixing is needed on the last (Mg, Y) sublattice. The primary solidification region of τ-phase could be obtained by the following model:

$$(Al, Mg, Y)_8: (Al, Mg, Y)_1: (Al, Mg, Y)_{1.6}: (Mg, Y)_{1.4}$$

A combination of the first two lattices is allowed to reduce the number of the end members. This yields:

$$(Al\%, Mg, Y)_9: (Al, Mg\%, Y)_{1.6}: (Mg, Y\%)_{1.4}$$

This model gives a good agreement with the primary solidification region which was obtained by [54] and provides homogeneity in the composition range of $0 \leq X_{Al} \leq 0.877$, $0 \leq X_Y \leq 1$, and $0 \leq X_{Mg} \leq 1$, which includes the Al_4MgY compound, since the composition of Al_4MgY is 66.7 at.% Al, 16.7 at.% Mg and 16.7 at.% Y which is covered by the composition range of this model.

The melting point of τ-phase is reported only by Odinaev and Ganiev [54] around 780°C; however in this calculation it is evaluated as 1085°C. It was difficult to reproduce the experimental region while maintaining its melting point at 820°C.

Based on the established model for τ-phase, the Gibbs energy per mole of formula unit can be represented by the following equation:

$$
\begin{aligned}
G_m^{Al_4MgY} &= y_{Al}^{I} y_{Al}^{II} y_{Mg}^{III\,0} G_{Al:Al:Mg}^{Al_4MgY} + y_{Al}^{I} y_{Mg}^{II} y_{Mg}^{III\,0} G_{Al:Mg:Mg}^{Al_4MgY} + y_{Al}^{I} y_{Y}^{II} y_{Mg}^{III\,0} G_{Al:Y:Mg}^{Al_4MgY} \\
&+ y_{Al}^{I} y_{Al}^{II} y_{Y}^{III\,0} G_{Al:Al:Y}^{Al_4MgY} + y_{Al}^{I} y_{Mg}^{II} y_{Y}^{III\,0} G_{Al:Mg:Y}^{Al_4MgY} + y_{Al}^{I} y_{Y}^{II} y_{Y}^{III\,0} G_{Al:Y:Y}^{Al_4MgY} \\
&+ y_{Mg}^{I} y_{Al}^{II} y_{Mg}^{III\,0} G_{Mg:Al:Mg}^{Al_4MgY} + y_{Mg}^{I} y_{Mg}^{II} y_{Mg}^{III\,0} G_{Mg:Mg:Mg}^{Al_4MgY} + y_{Mg}^{I} y_{Y}^{II} y_{Mg}^{III\,0} G_{Mg:Y:Mg}^{Al_4MgY} \\
&+ y_{Mg}^{I} y_{Al}^{II} y_{Y}^{III\,0} G_{Mg:Al:Y}^{Al_4MgY} + y_{Mg}^{I} y_{Mg}^{II} y_{Y}^{III\,0} G_{Mg:Mg:Y}^{Al_4MgY} + y_{Mg}^{I} y_{Y}^{II} y_{Y}^{III\,0} G_{Mg:Y:Y}^{Al_4MgY} \\
&+ y_{Y}^{I} y_{Al}^{II} y_{Mg}^{III\,0} G_{Y:Al:Mg}^{Al_4MgY} + y_{Y}^{I} y_{Mg}^{II} y_{Mg}^{III\,0} G_{Y:Mg:Mg}^{Al_4MgY} + y_{Y}^{I} y_{Y}^{II} y_{Mg}^{III\,0} G_{Y:Y:Mg}^{Al_4MgY} \\
&+ y_{Y}^{I} y_{Al}^{II} y_{Y}^{III\,0} G_{Y:Al:Y}^{Al_4MgY} + y_{Y}^{I} y_{Mg}^{II} y_{Y}^{III\,0} G_{Y:Mg:Y}^{Al_4MgY} + y_{Y}^{I} y_{Y}^{II} y_{Y}^{III\,0} G_{Y:Y:Y}^{Al_4MgY} \\
&+ RT(0.75 \sum_{i=Al}^{Y} y_i^{I} \ln y_i^{I} + 0.13 \sum_{i=Al}^{Y} y_i^{II} \ln y_i^{II} + 0.12 \sum_{i=Mg}^{Y} y_i^{III} \ln y_i^{III}) \\
&+ y_{Al}^{I} y_{Mg}^{I} y_{Y}^{I} (y_{Al}^{II\,0} L_{Al,Mg,Y:Al/Mg/Y:Mg/Y}^{Al_4MgY} + y_{Mg}^{II} y_{Mg}^{III\,0} L_{Al,Mg,Y:Al/Mg/Y:Mg/Y}^{Al_4MgY} \\
&+ y_{Y}^{II} y_{Y}^{III\,0} L_{Al,Mg,Y:Al/Mg/Y:Mg/Y}^{Al_4MgY}) + y_{Al}^{II} y_{Mg}^{II} y_{Y}^{II} (y_{Al}^{I\,0} L_{Al,Mg,Y:Al/Mg/Y:Mg/Y}^{Al_4MgY} \\
&+ y_{Mg}^{II} y_{Mg}^{III\,0} L_{Al,Mg,Y:Al/Mg/Y:Mg/Y}^{Al_4MgY} + y_{Y}^{II} y_{Y}^{III\,0} L_{Al,Mg,Y:Al/Mg/Y:Mg/Y}^{Al_4MgY}) \\
&+ y_{Mg}^{III} y_{Y}^{III} (y_{Al}^{I} y_{Al}^{II\,0} L_{Al/Mg/Y:Al/Mg/Y:Mg,Y}^{Al_4MgY} + y_{Mg}^{I} y_{Mg}^{II\,0} L_{Al/Mg/Y:Al/Mg/Y:Mg,Y}^{Al_4MgY} \\
&+ y_{Y}^{I} y_{Y}^{II\,0} L_{Al/Mg/Y:Al/Mg/Y:Mg,Y}^{Al_4MgY}) \qquad (5.1)
\end{aligned}
$$

$y_{Al/Mg/Y}^{I}$, $y_{Al/Mg/Y}^{II}$, $y_{Mg/Y}^{III}$ are the site fractions of the first sublattice, second sublattice, and third sublattice, respectively. The (/) sign is used here for the interchangeable constituents in the same sublattice to make the equation shorter.

The optimized parameters are listed in Table 5.2. Three G and one L parameters were used to reproduce the experimental primary solidification region of τ-phase.

Table 5.2: *Ternary interaction parameters with the τ -phase parameters.*

Ternary terms for the liquid	**a (J.mole^{-1} per formula unit)**	**b (J.mole^{-1}K)**
L_0(Mg, Al, Y)	-150 000	0
L_1(Mg, Al, Y)	-180 000	0
G (Al: Mg: Y)	-25 000	8.41
G(Al: Al: Y)	-21 000	5.3
G(Al: Y: Mg)	-26 000	4.4
L (Al, Mg, Y: Al: Mg; 0)	-96 000	4

To obtain a better agreement with the experimental liquidus isotherms, two ternary interaction terms were added to the description of the liquid phase. These parameters along with the model parameters of τ–phase are listed in Table 5.2. The resulting ternary phase diagram in comparison with the experimental results from the literature is shown in Figure 5.3. The ternary phase diagram of the Mg-Al-Y system was obtained in detail by projecting liquidus lines from isothermal sections at 100°C temperature steps on the Gibbs triangle.

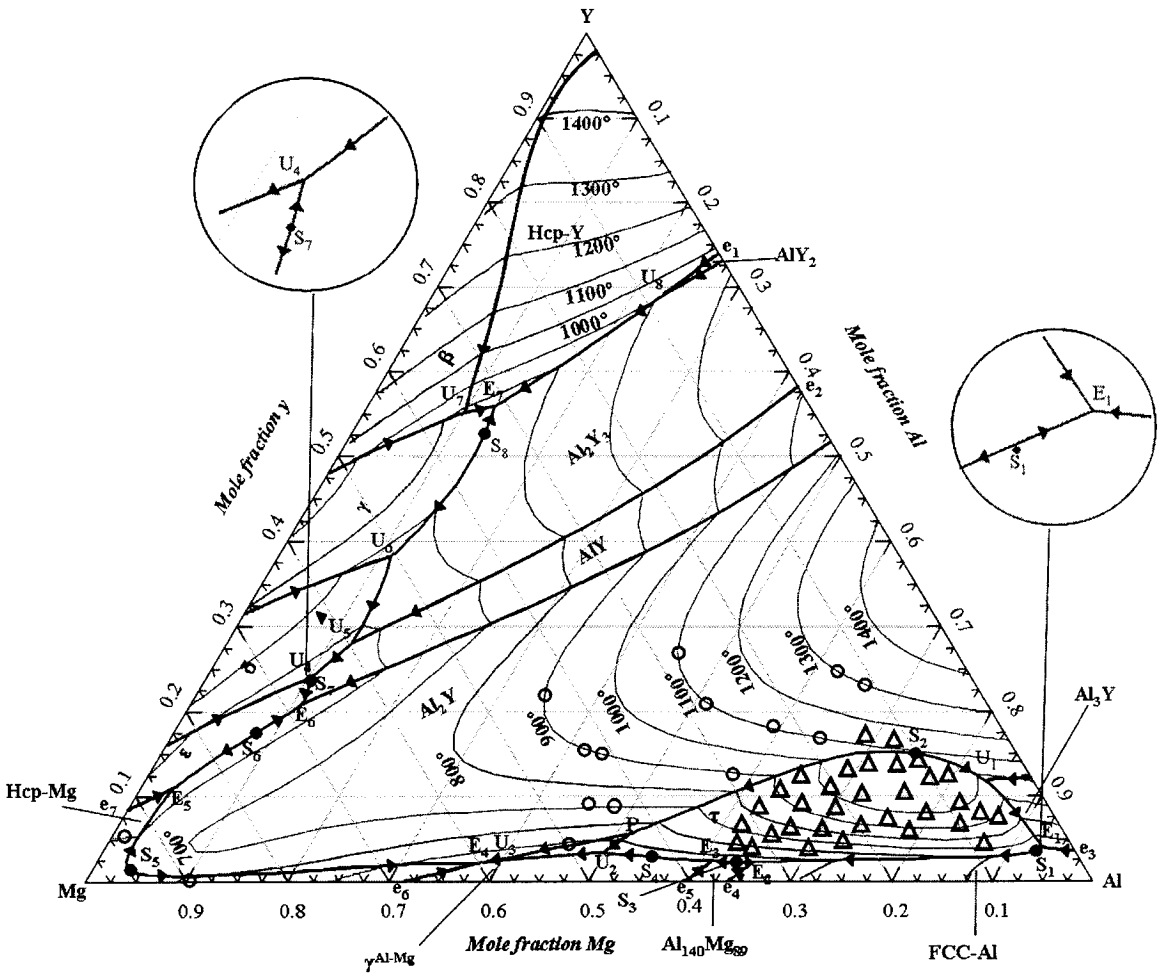

Figure 5.2: *The calculated Al-Mg-Y ternary phase diagram with the invariant points, ○-experimental liquidus isotherms, △-Primary solidification region for τ-phase [54]*

In this system, 16 ternary four-phase-equilibria points are determined; 7 ternary eutectic points, 8 ternary quasi peritectic points, and one ternary peritectic point as can be seen in Table 5.3. Moreover, it involves 15 ternary three-phase-equilibria points; 8 saddle points, and 7 binary eutectic points as listed in Table 5.4.

Table 5.3: *Calculated 4-phase equilibria points and their reactions in the Al-Mg-Y system compared with the experimental data from the literature.*

#	Reaction	Calculated (this work)					Experimental [54]			
		T(°C)	Type	at.%			T(°C)	at.%		
				Al	Mg	Y		Al	Mg	Y
1	Liquid ⇆ τ + Al_3Y + Fcc-Al	612.8	E_1^*	93	3	4				
2	Liquid ⇆ Fcc-Al + $Al_{140}Mg_{89}$ + τ	431.4	E_2	65.2	32.7	2.1	440	63.6	35.5	0.9
3	Liquid ⇆ $Al_{140}Mg_{89}$ + τ + $\gamma^{Al\text{-}Mg}$	430.5	E_3	61	36.7	2.3	430.5	57	42.2	0.8
4	Liquid ⇆ $\gamma^{Mg\text{-}Y}$ + Al_2Y + Hcp-Mg	419.6	E_4	37.6	60.4	2	438	29.3	67.7	3
5	Liquid ⇆ Al_2Y + Hcp-Mg + ε	538.5	E_5^*	3.3	85.6	1.1				
6	Liquid ⇆ Al_2Y + ε + AlY	817.5	E_6^*	11	68	21				
7	Liquid ⇆ Al_2Y_3 + $\gamma^{Mg\text{-}Y}$ + Hcp-Y	727	E_7^*	12.7	31.4	55.9				
8	Liquid + Al_2Y ⇆ τ + Al_3Y	969.1	U_1	83.4	4.7	11.9	750	83	4.2	12.8
9	Liquid + τ ⇆ $\gamma^{Mg\text{-}Y}$ + Al_3Y	434.6	U_2^*	50	47	3				
10	Liquid + Al_3Y ⇆ $\gamma^{Mg\text{-}Y}$ + Al_2Y	693.8	U_3^*	37.6	60.4	2				
11	Liquid + δ ⇆ ε + AlY	549.7	U_4^*	10.3	65.6	24.1				
12	Liquid + Al_2Y_3 ⇆ AlY + δ	575.3	U_5^*	12.3	59.6	28.1				
13	Liquid + $\gamma^{Mg\text{-}Y}$ ⇆ δ + Al_2Y_3	652	U_6^*	11	50.7	38.3				
14	Liquid + β-Y ⇆ $\gamma^{Mg\text{-}Y}$ + Hcp-Y	771.4	U_7^*	10.1	34.7	55.2				
15	Liquid + AlY_2 ⇆ Al_2Y_3 + Hcp-Y	908.7	U_8^*	23	8	69				
16	Al_2Y + τ ⇆ Liquid + Al_3Y	531.6	P^*	51.4	43	5.6				

* ***Predicted for the first time.***

***Table* 5.4:** Calculated 3-phase equilibria points and their reactions in the Al-Mg-Y system compared with the experimental data from the literature.

#	Reaction	Calculated (this work)					Experimental [54]			
		T(°C)	Type	at.%			T(°C)	at.%		
				Al	Mg	Y		Al	Mg	Y
1	Liquid ⇆ τ + Fcc-Al	613.9	S_1	92.6	3.8	3.6	589	88	6.2	5.8
2	Liquid ⇆ Al_2Y + τ	1088.6	S_2	75	10	15	590	68.1	13.2	18.7
3	Liquid⇆ $Al_{140}Mg_{89}$+τ	432	S3	63.5	34.3	2.2	441	60.8	37.5	1.8
4	Liquid ⇆ τ+ $\gamma^{Mg\text{-}Y}$	439.3	S4	54.8	42.4	2.8	447	44.5	52.5	3
5	Liquid ⇆ Al_2Y+ Hcp-Mg	625	S6	3.8	94.9	1.3	594	13.2	80	6.8
6	Liquid ⇆ Al_2Y+ε	547.6	S8*	8.2	74.3	17.5				
7	Liquid ⇆ ε+AlY	549.8	S9*	10.4	66	23.6				
8	Liquid ⇆ Al_2Y_3+ $\gamma^{Mg\text{-}Y}$	730.7	S10*	13.3	34	52.7				
9	Liquid ⇆ AlY_2+ Hcp-Y	967.3	e1	26	0	74				
10	Liquid ⇆ AlY+Al_2Y_3	1087.4	e2	43	0	57				
11	Liquid ⇆ Al-Fcc-+Al_3Y	640	e_3	97.5	0	2.5	637	96.9	0	3.1
12	Liquid ⇆Fcc-Al+$Al_{140}Mg_{89}$	449.3	e_4	63.8	36.2	0	450	62.5	37.4	0
13	Liquid ⇆$Al_{140}Mg_{89}$+ $\gamma^{Mg\text{-}Y}$	450	e_5	59.6	40.4	0	450	58.5	41.5	0
14	Liquid⇆ $\gamma^{Mg\text{-}Y}$ +Hcp-Mg	430.3	e_6	31.7	68.3	0	438	30	70	0
15	Liquid ⇆Hcp-Mg+ε	558.4	e_7	0	91.6	8.4				

**** Predicted for the first time.***

The calculated 4 and 3-phase equilibria points show a good agreement with the available experimental data reported by [54] as shown in Tables 8 and 9. However, the calculated temperature of U1 and S2 points show a discrepancy with the experimental data. This contradiction is due to the fact that the liquidus around τ-phase was predicted to be higher than what Odinaev and Ganiev [54] reported. Such a low liquidus in this region is very difficult to reproduce because of the high enthalpies and quite normal entropies of formation of the binary Al-Y intermetallic phases Al_3Y, Al_2Y, AlY, Al_2Y_3,

and AlY_2. These high liquidus temperatures were observed by other researchers who studied similar systems (i.e Mg-Al-RE) [69,70,71] Further, the existence of Al_4Y which was not included in this work and was considered by [54] may have contributed to this inconsistency. It is worth emphasizing that the most recent works [18,19,23] on Al-Y did not consider Al_4Y a stable phase in this system.

A reasonable agreement has also been achieved with the experimental work of Drits *et al.* [52] as shown in Figure 5.3.

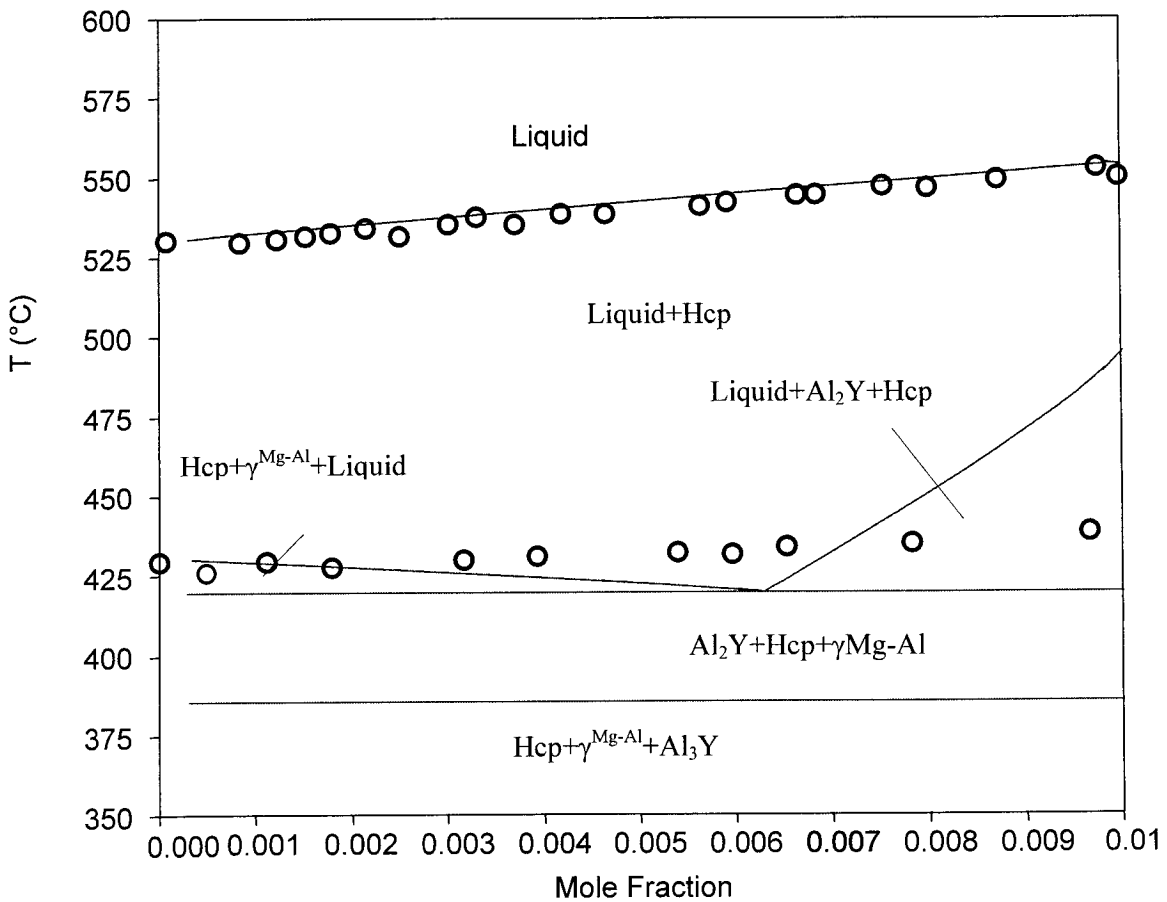

(a)

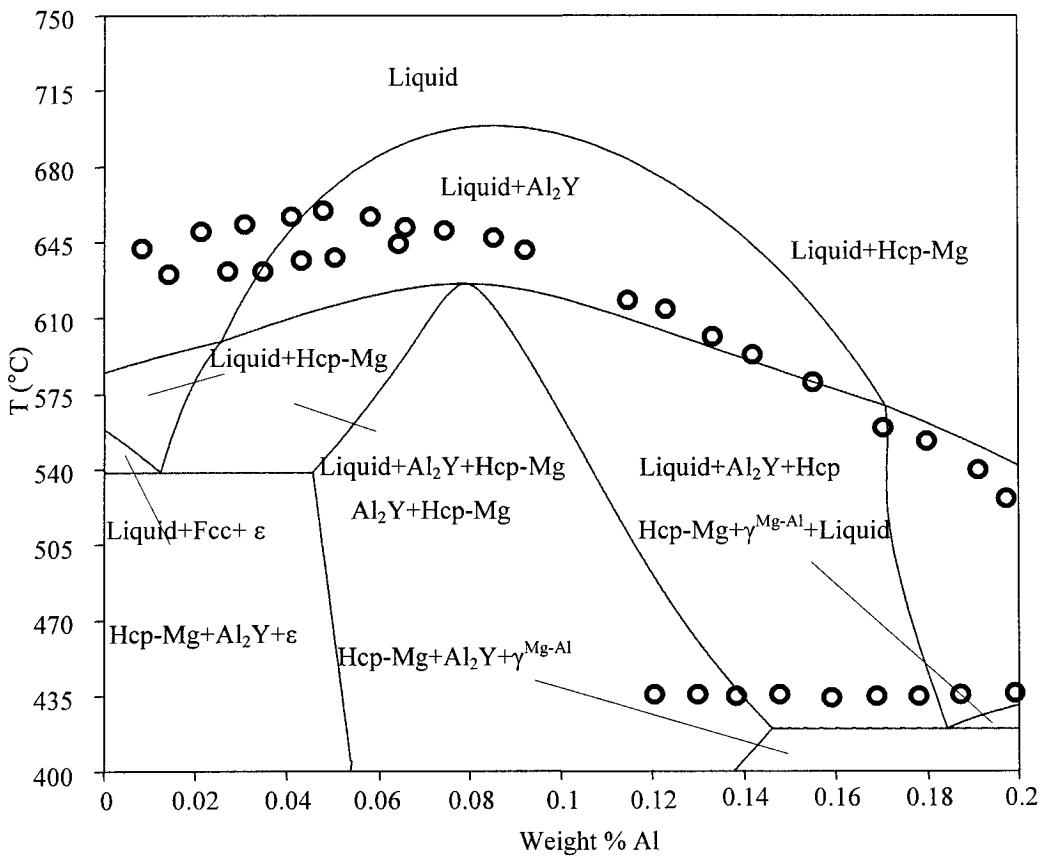

(b)

Figure 5.3: *The calculated vertical sections for 80 wt% Mg compared with experimental data from the literature (a) 0-1 at.%Y, and (b) 0-20 wt% Al.*

Figure 5.3(a) shows that the experimental data of Drits *et al.* [52] has higher temperature than the calculated one especially in the regions where ε-phase exists. This is due to the high melting point of ε-phase, 633°C, reported by Drits *et al.* [52]. However; in the current work this was evaluated as 614°C which is in good agreement with [42].

For a better understanding, the ternary Al-Mg-Y liquidus surface is drawn in 3-D, with the temperature color key, from the evaluated thermodynamic model using GRAPHIS software [72] as shown in Figure 5.4. as sample calculated data which was used to draw this surface are tabulated in appendix, knowing that the number of calculated points by which the liquidus surface was generated is around 25 000 data points.

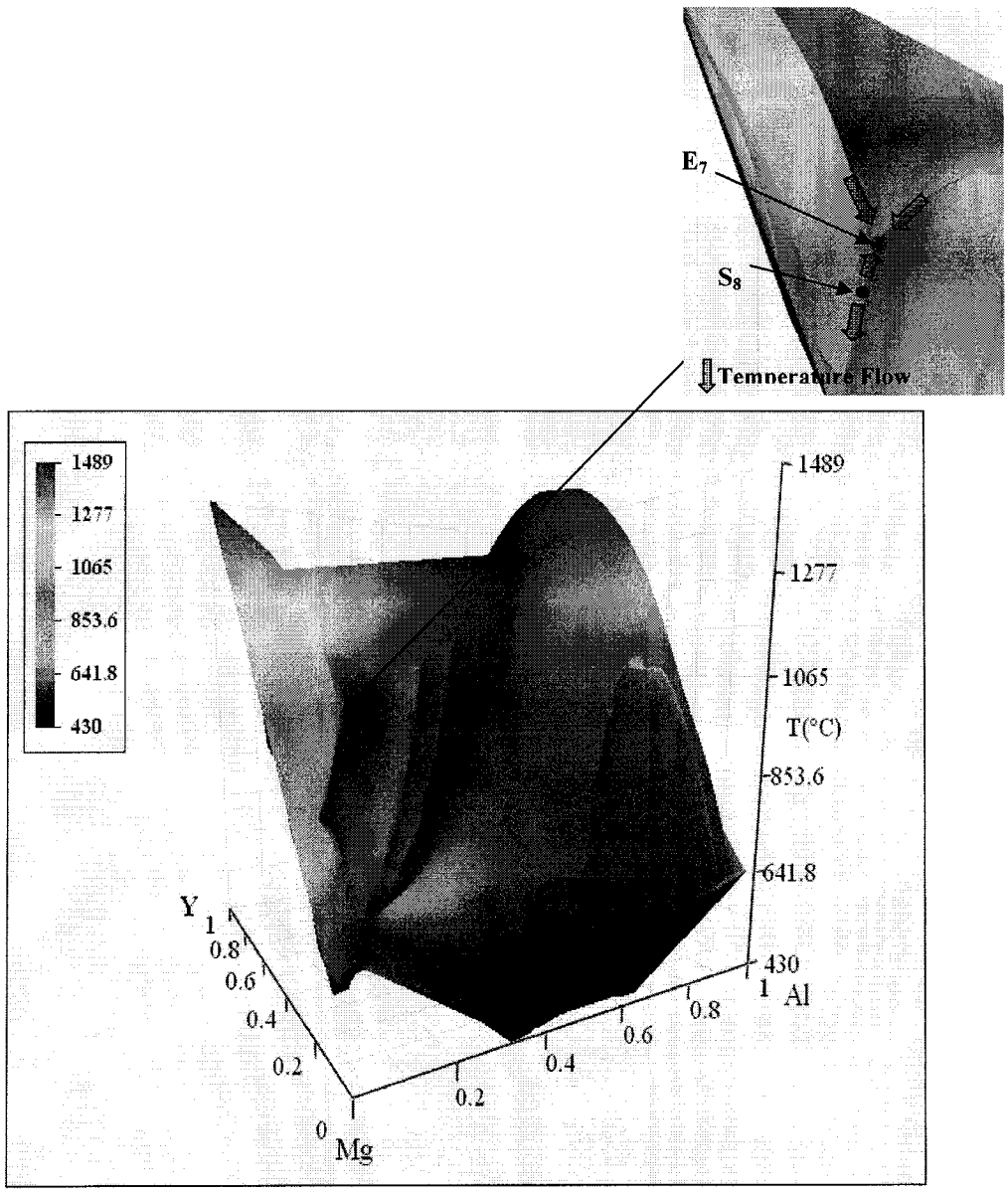

Figure 5.4: *The liquidus surface of the Al-Mg-Y system in 3D with color key which indicates the temperature range.*

CHAPTER6

SUMMARY AND FUTURE WORK

6.1 Summary and Original Contributions

The major accomplishments and contributions achieved in the present study can be summarized as follows:

i. A thermodynamic model for the entire composition range of the ternary Mg-Al-Y has been established for the first time in this work.

ii. The phase relations and thermodynamic descriptions of the Al-Y, and Mg-Y systems were obtained using optimization with the phase equilibria and thermodynamic experimental data from the literature. A consistent set of thermodynamic parameters were derived in this work. These parameters were used to calculate the thermodynamic description of the ternary Mg-Al-Y. The results of the calculations were compared with the experimental data from the related literature.

iii. The database for the ternary Mg-Al-Y system was constructed using the Redlich-Kister polynomial model for all the disordered phases, sublattice model for the non-stoichiometric compounds, and the stoichiometric model for the linear

compounds. All of these phases were evaluated without adding any lattice stability values to the pure components.

iv. One ternary non stoichiometric compound was included in this assessment of the Mg-Al-Y ternary system. Its Gibbs energy was evaluated using the sublattice model and in order to obtain a good agreement with the experimental liquidus isotherms two ternary interaction parameters were added to the description of the liquid phase.

v. A good agreement with the experimental data has been achieved for the calculated binary systems and their thermodynamic properties, the liquidus isotherms, the primary solidification region for τ-phase, and for the calculated vertical sections in the ternary Mg-Al-Y system.

vi. The predicted invariant points in the Mg-Al-Y system were 16 ternary four–phase-equilibria points; 7 ternary eutectic points, 8 ternary quasi peritectic points, and one ternary peritectic point. Further, 15 ternary three-phase-equilibria points were determined; 8 saddle points, and 7 binary eutectic points.

vii. The constructed Mg-Al-Y database forms a basis for further developments in this system and allows the researchers to carry out key experiments towards finding the Mg-Al-Y alloys with optimum mechanical properties for industrial applications.

viii. The ternary Mg-Al-Y system is a part of the development of a multicomponent Mg-Al base alloy database and can be used for higher order systems.

6.2 Future Work

- The current understanding for the equilibria in the Mg-Al-Y system should be verified using key experiments combined with computational thermodynamics.

- The constructed database can be used as a road map for the development of new alloys in this system and for better understanding of the existing ones.

- More experimental and computational work is needed for the thermodynamic properties of the ternary Mg-Al-Y system.

- Advanced optimization techniques such as genetic algorithms should be applied to phase diagram calculation in order to correlate the uncertainties in the experimental values with the optimized parameters.

REFERENCES

[1] D.R. Gaskell, Introduction to the Thermodynamics of Materials, Taylor and Francis, 3rd Edition, 1995.

[2] U.R. Kattner, "The Thermodynamic Modeling of Multicomponent Phase Equilibria", JOM, 49(12), 1997, 14-19.

[3] Y. Austin Chang, S. Chen, F. Zhang, X. Yan, F. Xie, R. Schmid-Fetzer, W. Alan Oatese, "Phase Diagram Calculation: Past. Present and Future",Progress in material science, 49,2004,.313-345.

[4] "Pandat TM 4.0: Multi-Component Phase Diagram Calculation Software" 2000-2003, Computherm LLC, Madison WI, U.S.A.

[5] www.tulane.edu/~sanelson/geol212/ternaryphdiag.htm.

[6] S. Stølen, T. Grande, Chemichal Thermodynamics of Material, John Wiley & Sons, February. 2004.

[7] L. Gaines,R. Cuenca, F. Stodolsky, and S. Wu, "Potential Applications of Wrought, "Magnesium Alloys for Passenger Vehicles," presented at the ATD-CCM, Detroit, MI, Oct. 1995, 24-28.

[8] E. Ghali; W. Dietzel; K-U. Kainer, "Testing of General and Localized Corrosion of Magnesium Alloys: A Critical Review", Journal of Materials Engineering and Performance, 13(5), 2004, 517-529.

[9] N.V. Ravi Kumar, J.J. Blandin, M. Suery, E. Grosjean, "Effect of alloying elements on the ignition resistance of magnesium alloys", Scripta Materialia 49 ,2003, 225–230.

[10] M. Socjusz-Podosek, L. Lity nska, "Effect of yttrium on structure and mechanical properties of Mg alloys", Materials Chemistry and Physics 80, 2003, 472–475.

[11] M. Suzuki, H.Sato, K.Maruyama, H. Oikawa,"Creep behavior and deformation microstructures of Mg–Y alloys at 550 K", Materials Science and Engineering, 252, 1998, 248–255.

[12] M O. Pekguleryuz, J. Renaud, "Creep Resistance in Mg-Al-Ca Casting alloys", 2000 TMS Annual Meeting & Exhibition, held in Nashville, Tennessee, March 12-March 15, 2000, 279-284.

[13] LM. Petrova, VV. Krasnoyarskii, "The Effect of Phase Composition on Corrosion Behavior of Mg-Y-Al Alloys", Protection of Metals, 31(4), 1995, 398-400. Translated from Zashchita Metallov, 31(4), 1995, 438-440.

[14] L.L. Rokhlin, "Magnesium Alloys Containing Rrare Earth Metals Structure and Properties, Baikove Instituate of Metalluargy and Materials Science, Moscow, Russia. tylor & Francis inc, 2003.

[15] I. Ansara, A. T. Dinsdale, and M. H. Rand, "COST507 – Thermochemical database for light metal alloys", European Commission EUR 18499, 1998.

[16] K.C. Hari kumar, P. Wollants, "Some Guidelines for Thermodynamic Optimization of Phase Diagrams" Journal of Alloys and Compounds, 320, 2001, 189-198.

[17] E.M. Savitskii, V.F. Terekhova, " Study of Rare Metals and Alloys", I. P. Bardin Razvit. Metall. SSSR,1976, 240-57.

[18] R.L. Snyder, "Yttrium-Aluminum Alloy Studies", Master's Thesis, Iowa State University for Science and Technology AMES, Iwoa,1960.

[19] C.E. Lundin, Jr D.T. Klodt, "Phase Equilibria in The Yttrium-Aluminum System", Trans. Quart, 54(2),1961, 68-75.

[20] M.E. Drits, E.S. Kadaner, and N.D. Shoa, "Structure and Properties of Aluminum-Rich Al-Y Alloys", Izvestiya Akademii Nauk SSSR, Metally, 6,1969, 150-153.

[21] KA. Jr. Gschneidner, F.W. Calderwood, "The Al-Y (Aluminum-Yttrium) System", Bulletin of Alloy Phase Diagrams, 10(1), 1989, 44-47.

[22] P.I. Kripyakevich, "The Crystal Structure of YAl_2", Kristallografiya, 5, 1960, 463-464.

[23] C. Rongzhen, W. Xiangzhong; L. Jingqi, "The Isothermal Section of the Phase Diagram of the Ternary System Al-Sn-Y at Rroom Temperature", Journal of Alloys and Compounds, 218(2), (1995), 221-223.

[24] Z. Lingmin, W. Shouyu, "The 800 K Isothermal Section of the Y-Al-Sb Phase Diagram" Journal of Alloys and Compounds, 351(1-2), (2003), 176-179.

[25] A. Chelkowski, E. Talik, J. Szade, J. Heimann, A. Winiarska, A. Winiarski, "Solid Solubility of Rare Earths in Aluminum", Journal of the Less-Common Metals 141(2), 1988, 213-216.

[26] R. Richter, Z. Altounian, J.O. Strom-Olsen, U. Koester, M. Blank-Bewersdorff, "Y_5Al_3; A New Yttrium-Aluminum Compound", Journal of Materials Science 22(8), 1987 2983-2986.

[27] D.M. Bailey, "Structures of Two Polymorphic Forms of YAl_3", Acta Crystallographica, 23(5), 1967, 729-733.

[28] R. Raggio, G. Borzone, R. Ferro, "The Al-Rich Region in the Y-Ni-Al System:

microstructures and phase equilibria", Intermetallics ,8(3), 2000, 247-257.

[29] Yu. O. Esin,, P.V. Gel'd, M.S. Petrushevskii, N.P. Bobrov, G.M. Ryss, V.V. Sokolov, I.P. Pazdnikov, A. Ya. Dubrovskii,, "Enthalpies of Formation of Molten Binary Aluminum Alloys with Yttrium, Zirconium, Vanadium, and Chromium", v sb., Splavy Redk. Met. s Osobymi Fiz.-khim. Svoistvami 1975, 177-180.

[30] G.M. Ryss, Yu.O. Esin, A.I. Stroganov, P.V. Gel'd, "Enthalpies of Formation of Yttrium- Aluminum Molten Alloys", Zhurnal Fizicheskoi Khimii, 50(4), 1976, 985-986.

[31] V.I. Kober, I.F. Nichkov, S.P. Raspopin, V.N. Nauman, Izv, " Composition and Thermodynamic Properties of Yttrium-Aluminum System", Tsvetnaya Metallurgiya, 5, 1979, 40-43.

[32] G.N. viadadze, A.A. Petrov, E.K. Kazenas,, "Thermodynamics of the Vacuum Evaporation of Alloys of Scandium, Yttrium, Lanthanum, and Neodymium with Aluminum" Protsessy Tsvetn. Metall. Nizk. Davleniyakh, 1983, 94-98.

[33] J. Gröbner, H. Lukas, F. Aldinger, "Thermodynamic calculations in the Y-Al-C System", Journal of Alloys and Compounds, 220(1-2), 1995, 8-14.

[34] V.S Timofeev, A.A. Turchanin, A.A. ZubkoVl", I.A. Tomilin, "Enthalpies of Formation for the Al-Y and Al-Y-Ni Intermetallic Compounds", Thermochimicha acta 299, 1997, 37-41.

[35] G. Borzone, A. Cicciolia, P.L. Cigninia, M. Ferrinia, D. Gozzia, "Thermodynamics of the YA1-YAl_2 System", Intermetallics, 8, 2000, 203-212.

[36] M.S. Petrusheveskii, G.M. Ryss, " Calculations of the Activities of Components in Liquid Binary Alloys of Yttrium with Aluminum and Silicon", 60(6), 1986, 1532-1535.

[37] V.K. Kulifeev, V.N. Kaplenkov, "Thermodynamics of the Interaction in the System Yttrium- Aluminum", Nauch. Tr. Mosk. In-t Stali i Splavov 131, 1981, 110-112.

[38] Z.A. Sviderskaya, E.M. Padezhnova, " Phase Equilibriums in Magnesium-Yttrium and Magnesium-Yttrium-Manganese Systems", Izvestiya Akademii Nauk SSSR, Metally 6, 1968, 183-190.

[39] E. D Gibson, O. N. Carlson, "The Yttrium-Magnesium Alloy System", Transactions of the American Society for Metals 52, 1960, 1084-1096.

[40] T.B Massalski "Binary Alloy Phase diagrams", Second Edition, Puplisher William W.scott, Jr., 1990, 1-3.

[42] J. F Smith, D.M. Bailey, D.B. Novotny, J.E. Davison, " Thermodynamics of Formation of Yttrium-Magnesium Intermediate Phases", Acta Met. 13(8), 1965,

889-895.

[43] H. Flandorfer, M. Giovannini, A. Saccone, P. Rogl, R. Ferro, "The Ce-Mg-Y System", Physical Metallurgy and Materials Science 28A(2), 1997, 265-276.

[44] M.-X. Zhang, P.M. Kelly, " Edge-to- edge matching and it's applications PartII. Application to Mg-Al, Mg-Y, and Mg-Mn Alloys", Acta Materialia, 53, 2005, 1085-1096.

[45] R. Agarwal, H. Feufel, F. Sommer, "Calorimetric Measurements of Liquid La-Mg, Mg-Yb and Mg-Y Alloys", Journal of Alloys and Compounds 217(1),1995, p.59-64.

[46] O.B. Fabrichnaya, H.L. Lukas, G. Effenberg, F. Aldinger, "Thermodynamic Optimization in the Mg-Y System", Intermetallics 11(11-12), 200, 1183-1188.

[47] Ganesan, V.Schuller, F. Feufel, H. Sommer, F. Ipser, Herbert. "Thermodynamic Properties of Ternary Liquid Cu-Mg-Y Alloys", Zeitschrift fuer Metallkunde 88(9), 1997, 701-710.

[48] V. Ganesan, H. Ipser, " Thermodynamic Properties of Liquid Magnesium-Yttrium Alloys", Journal de Chimie Physique et de Physico-Chimie Biologique 94(5), 1997, 986-991.

[49] Q. Ran, H.L. Lukas, Effenberg G, G. Petzow, " Thermodynamic Optimization of the Magnesium-Yttrium System", CALPHAD: Computer Coupling of Phase Diagrams and Thermochemistry, 12(4), 1988, 375-381.

[50] I.N. Pyagai, E.Z Khasanova, A.V. Vakhobov, O.V. Zhikhareva, " Heat of Formation of the Intermetallic Compound Magnesium Ytterbium (Mg_2Yb) at 298 K", Doklady Akademii Nauk Tadzhikskoi SSR 33(9), 1990, 602-604.

[51] T. Thangarajah, "Thermodynamic Modeling of the Mg-Al-Sb System", Masters thesis, Concordia University 2004.

[52] M.E. Drits, E.M. Padezhnova, T.V. Dobatkina, "Phase Equilibriums in Magnesium-Yttrium-Aluminum Alloys", Izvestiya Akademii Nauk SSSR, Metally 3, 1979, 223-227.

[53] O.S. Zarechnyuk, M.E. Drits, R.M Rykhal, V.V. Kinzhibalo, "Study of a Magnesium-Aluminum-Yttrium System at 400 in the Phase Containing 0-33.3 at.% Yttrium", Izvestiya Akademii Nauk SSSR, Metally, 5, 1980, 242-244.

[54] Kh. O. Odinaev, I.N. Ganiev, " Quasibinary Sections and Liquidus Surface of the Aluminum-Magnesium-Yttrium Aluminide (YAl_2) System", Izvestiya Vysshikh Uchebnykh Zavedenii, Tsvetnaya Metallurgiya, 6, 1990, 90-95.

[55] Kh. O. Odinaev, I.N. Ganiev, V.V Kinzhibalo, Kh.K. Kurbanov, "Phase Equilibria in Aluminum-Magnesium-Yttrium and Aluminum-Magnesium-Cerium Systems at 673 K" Izvestiya Vysshikh Uchebnykh Zavedenii, Tsvetnaya Metallurgiya, 4, 1989, 75-77.

[56] L. Kaufman and H. Bernstein, Computer Calculation of Phase Diagrams, Academic Press, New York, 1970. (Cited in [3]).

[57] G. Eriksson, K. Hack, Metall Trans B 1990:21B:1013. (Cited in [3]).

[58] VT. Thompson, G. Eriksson, CW. Bale. AD. Pelton, "Applications of F*A*C*T in High Temperature Materials Chemistry". Electrochemical Society. Inc (USA) 1997: 16-30. (Cited in [3]).

[59] Y. M. Muggianu, M. Gambino, J. P. Bross, "Enthalpies of formation of liquid alloys bismuth-gallium-tin at 723.deg.K. Choice of an analytical representation of integral and partial excess functions of mixing", J. Chimie Physique 72(1), 1975, 83-88.

[60] A. Dinsdale, "Thermodynamic data of the elements", CALPHAD, 15, 1991, 317-325.

[61] O. Redlich, A.T. Kister, "Thermodynamics of Nonelectrolyte Solutions, X-Y-T Relations in a Binary System", Journal of Industrial and Engineering Chemistry Washington D. C., 40, 1948, 341-345.

[62] M. Hillert, "Empirical Methods of Predicting and Representing Thermodynamic Properties of Ternary Solution Phases", Calphad 4(1), 1980, 1-2.

[63] P. Chartrand, AD. Pelton, "On The Choice of "Geometric" Thermodynamic Models", Journal of Phase Equilibria, 21(2), 2000, 141-147.

[64] Q. Ran, H.L. Lukas, G. Effenberg, G. Petzow, " A Thermodynamic Optimization of the Aluminum-Yttrium System", Journal of the Less-Common Metals 1989, 213-222.

[65] A.R. Miedema, "On the Heat of Formation of Solid Alloys", Journal of the Less-Common Metals, 46(1), 1976, 67-83.

[66] K.C. Hari Kumar, I. Ansara, P. Wollants, "Sublattice Modeling of the μ-phase", Calphad, 22(3), 1998, 323-334.

[67] P. Villars, L.D. Calvert, "Pearson Handbook of Hrystallographic Data for Intermetallic Phases", 1991.

[68] "Powder Cell for windows", Version 1.0, 1997, W.Kraus & G. Nolze, Federal Institute for Materials Research and Testing, Rudower Chausse 5, 12489 Berlin, Germany.

[69] J. Grbner, R.Schmid-Fetzer, A. Pisch, G.Cacciamani, P. Riani, R. Ferro, "Experimental Investigation and Thermodynamic Calculation of the Al-Mg-Sc System", Z Metallkd, 90, 1999, pp 872-80.

[70] J. Grobner, D. Kervokov, R. Schmid-Fetzer, " Thermodynamic of Al-Gd-Mg Phase Equilibria Checked by Key Experiments", Z Metallkd, 92, 2001, pp 2-7.

[71] J. Grobner, D. Kervokov, R. Schmid-Fetzer, "Thermodynamic modeling of Al-Ce-Mg Phase Equilibria Coupled with Key Experiments" , Intermetallics, 10, 2002, pp 415-422.

[72] "Graphis graphing software for 2D and 3D data - high-quality scientific/engineering visualization for the Windows desktop", Version: 2.6.2, 2003, Kylebank Software Ltd.

APPENDIX

Sample of the calculated data which was used to draw the 3D surface are listed in the following table.

#	phaseName	T(°C)	x(Al)	x(Y)
1	Liquid+Fcc-Al	648.5	0.985	0.015
2	Liquid+Fcc-Al	648.5	0.984	0.015
3	Liquid+Fcc-Al	648.5	0.984	0.015
4	Liquid+Fcc-Al	648.5	0.983	0.014
5	Liquid+Fcc-Al	648.5	0.982	0.013
6	Liquid+Fcc-Al	648.5	0.981	0.012
7	Liquid+Fcc-Al	648.5	0.981	0.011
8	Liquid+Fcc-Al	648.5	0.98	0.011
9	Liquid+Fcc-Al	648.5	0.98	0.01
10	Liquid+Fcc-Al	648.5	0.979	0.01
11	Liquid+Fcc-Al	648.5	0.979	0.01
12	Liquid+Fcc-Al	648.5	0.979	0.009
13	Liquid+Fcc-Al	648.5	0.978	0.008
14	Liquid+Fcc-Al	648.5	0.978	0.007
15	Liquid+Fcc-Al	648.5	0.977	0.006
16	Liquid+Fcc-Al	648.5	0.976	0.005
17	Liquid+Fcc-Al	648.5	0.975	0.004
18	Liquid+Fcc-Al	648.5	0.975	0.002
19	Liquid+Fcc-Al	648.5	0.974	4E-04
21	Liquid+Fcc-Al	644.5	0.965	3E-04
22	Liquid+Fcc-Al	644.5	0.965	7E-04
23	Liquid+Fcc-Al	644.5	0.966	0.003
24	Liquid+Fcc-Al	644.5	0.967	0.004
25	Liquid+Fcc-Al	644.5	0.968	0.006
26	Liquid+Fcc-Al	644.5	0.968	0.007
27	Liquid+Fcc-Al	644.5	0.969	0.008
28	Liquid+Fcc-Al	644.5	0.969	0.008
29	Liquid+Fcc-Al	644.5	0.97	0.009
30	Liquid+Fcc-Al	644.5	0.97	0.01
31	Liquid+Fcc-Al	644.5	0.97	0.01
32	Liquid+Fcc-Al	644.5	0.971	0.01
33	Liquid+Fcc-Al	644.5	0.971	0.011
34	Liquid+Fcc-Al	644.5	0.972	0.012
35	Liquid+Fcc-Al	644.5	0.972	0.012
36	Liquid+Fcc-Al	644.5	0.973	0.013
37	Liquid+Fcc-Al	644.5	0.974	0.014
38	Liquid+Fcc-Al	644.5	0.975	0.016
39	Liquid+Fcc-Al	644.5	0.977	0.017
40	Liquid+Fcc-Al	644.5	0.979	0.019

41	Liquid+Fcc-Al	644.5	0.98	0.02
42	Liquid+Fcc-Al	644.5	0.98	0.02
44	Liquid+Fcc-Al	640	0.956	5E-04
45	Liquid+Fcc-Al	640	0.956	0.001
46	Liquid+Fcc-Al	640	0.956	0.003
47	Liquid+Fcc-Al	640	0.957	0.004
48	Liquid+Fcc-Al	640	0.958	0.006
49	Liquid+Fcc-Al	640	0.958	0.007
50	Liquid+Fcc-Al	640	0.959	0.008
51	Liquid+Fcc-Al	640	0.959	0.008
52	Liquid+Fcc-Al	640	0.959	0.009
53	Liquid+Fcc-Al	640	0.96	0.01
54	Liquid+Fcc-Al	640	0.96	0.01
55	Liquid+Fcc-Al	640	0.96	0.01
56	Liquid+Fcc-Al	640	0.961	0.011
57	Liquid+Fcc-Al	640	0.961	0.012
58	Liquid+Fcc-Al	640	0.962	0.012
59	Liquid+Fcc-Al	640	0.963	0.013
60	Liquid+Fcc-Al	640	0.964	0.014
61	Liquid+Fcc-Al	640	0.965	0.016
62	Liquid+Fcc-Al	640	0.966	0.017
63	Liquid+Fcc-Al	640	0.968	0.019
64	Liquid+Fcc-Al	640	0.97	0.021
65	Liquid+Fcc-Al	640	0.973	0.023
66	Liquid+Fcc-Al	640	0.975	0.024
67	Liquid+Fcc-Al	640	0.975	0.024
68	Liquid+Fcc-Al	640	0.975	0.024
70	Liquid+Fcc-Al	635.5	0.946	9E-04
71	Liquid+Fcc-Al	635.5	0.946	0.002
72	Liquid+Fcc-Al	635.5	0.947	0.004
73	Liquid+Fcc-Al	635.5	0.948	0.006
74	Liquid+Fcc-Al	635.5	0.948	0.007
75	Liquid+Fcc-Al	635.5	0.949	0.008
76	Liquid+Fcc-Al	635.5	0.949	0.008
77	Liquid+Fcc-Al	635.5	0.949	0.009
78	Liquid+Fcc-Al	635.5	0.95	0.01
79	Liquid+Fcc-Al	635.5	0.95	0.01
80	Liquid+Fcc-Al	635.5	0.95	0.01
81	Liquid+Fcc-Al	635.5	0.951	0.011
82	Liquid+Fcc-Al	635.5	0.951	0.012
83	Liquid+Fcc-Al	635.5	0.952	0.013
84	Liquid+Fcc-Al	635.5	0.953	0.014
85	Liquid+Fcc-Al	635.5	0.953	0.015
86	Liquid+Fcc-Al	635.5	0.955	0.016